Article

Phytocytokine signalling reopens stomata in plant immunity and water loss

https://doi.org/10.1038/s41586-022-04684-3

Received: 27 April 2021

Accepted: 24 March 2022

Published online: 4 May 2022

Check for updates

Zunyong Liu[1,9], Shuguo Hou[1,2,9]✉, Olivier Rodrigues[1,3], Ping Wang[1], Dexian Luo[1], Shintaro Munemasa[4], Jiaxin Lei[5], Jun Liu[1], Fausto Andres Ortiz-Morea[1], Xin Wang[6], Kinya Nomura[7,8], Chuanchun Yin[1], Hongbo Wang[2], Wei Zhang[6], Keyan Zhu-Salzman[5], Sheng Yang He[7,8], Ping He[1]✉ & Libo Shan[1]✉

Stomata exert considerable effects on global carbon and water cycles by mediating gas exchange and water vapour[1,2]. Stomatal closure prevents water loss in response to dehydration and limits pathogen entry[3,4]. However, prolonged stomatal closure reduces photosynthesis and transpiration and creates aqueous apoplasts that promote colonization by pathogens. How plants dynamically regulate stomatal reopening in a changing climate is unclear. Here we show that the secreted peptides SMALL PHYTOCYTOKINES REGULATING DEFENSE AND WATER LOSS (SCREWs) and the cognate receptor kinase PLANT SCREW UNRESPONSIVE RECEPTOR (NUT) counter-regulate phytohormone abscisic acid (ABA)- and microbe-associated molecular pattern (MAMP)-induced stomatal closure. SCREWs sensed by NUT function as immunomodulatory phytocytokines and recruit SOMATIC EMBRYOGENESIS RECEPTOR-LIKE KINASE (SERK) co-receptors to relay immune signalling. SCREWs trigger the NUT-dependent phosphorylation of ABA INSENSITIVE 1 (ABI1) and ABI2, which leads to an increase in the activity of ABI phosphatases towards OPEN STOMATA 1 (OST1)—a key kinase that mediates ABA- and MAMP-induced stomatal closure[5,6]—and a reduction in the activity of S-type anion channels. After induction by dehydration and pathogen infection, SCREW–NUT signalling promotes apoplastic water loss and disrupts microorganism-rich aqueous habitats to limit pathogen colonization. The SCREW–NUT system is widely distributed across land plants, which suggests that it has an important role in preventing uncontrolled stomatal closure caused by abiotic and biotic stresses to optimize plant fitness.

Plant genomes encode thousands of small peptides, the functions of which remain mostly unknown[7]. Some secreted peptides regulate plant development, reproduction, immunity and environmental adaptations, and function as short- and long-distance signalling molecules[7,8]. Plant peptides are usually perceived by cell-surface-resident receptor kinases[9,10]. Some receptor kinases function as pattern recognition receptors (PRRs) that recognize MAMPs or plant-derived damage-associated molecular patterns (DAMPs) and immunomodulatory phytocytokines[11–14]. The immune responses induced by MAMPs, DAMPs and phytocytokines collectively contribute to plant pattern-triggered immunity (PTI). The expression of phytocytokines is often induced after the perception of MAMPs by PRRs to boost plant immunity[13,14]. Some PRRs can perceive both phytocytokines and MAMPs, such as MALE DISCOVERER 1-INTERACTING RECEPTOR-LIKE KINASE 2 (MIK2), which recognizes SERINE-RICH ENDOGENOUS PEPTIDEs (SCOOPs) from plants and microorganisms[15,16]. How immunity is mechanistically coordinated by the concerted action of microbial patterns and host phytocytokines remains mostly unknown.

SCREWs function as phytocytokines

We analysed *Arabidopsis* transcriptome datasets for genes encoding small peptides (fewer than 120 amino acids (aa)) that are induced upon the perception of flg22, a 22-aa peptide that corresponds to the MAMP flagellin[17]. Three closely related genes, *AT1G06135*, *AT2G31345* and *AT1G06137*, were significantly upregulated at 30 and 60 min after flg22 treatment and were named *SCREW1*, *SCREW2* and *SCREW3*, respectively (Extended Data Fig. 1a). SCREWs contain an N-terminal signal peptide domain, a variable domain and a C-terminal conserved domain (Fig. 1a, Extended Data Fig. 1b). Phylogenetic analysis revealed an additional SCREW homologue, *AT2G31335* (*SCREW4*), in *Arabidopsis* (Fig. 1a, Extended Data Fig. 1b). The SCREW orthologues were detected in a

[1]Department of Biochemistry and Biophysics, Texas A&M University, College Station, TX, USA. [2]School of Municipal and Environmental Engineering, Shandong Jianzhu University, Jinan, China. [3]Unité de Recherche Physiologie, Pathologie et Génétique Végétales, Université Fédérale Toulouse Midi-Pyrénées, INP-PURPAN, Toulouse, France. [4]Graduate School of Environmental & Life Science, Okayama University, Okayama, Japan. [5]Department of Entomology, Texas A&M University, College Station, TX, USA. [6]Key Laboratory of Plant Development and Environmental Adaption Biology, School of Life Science, Shandong University, Qingdao, China. [7]Department of Biology, Duke University, Durham, NC, USA. [8]Howard Hughes Medical Institute, Duke University, Durham, NC, USA. [9]These authors contributed equally: Zunyong Liu, Shuguo Hou. ✉e-mail: hou_shuguo@126.com; pinghe@tamu.edu; lshan@tamu.edu

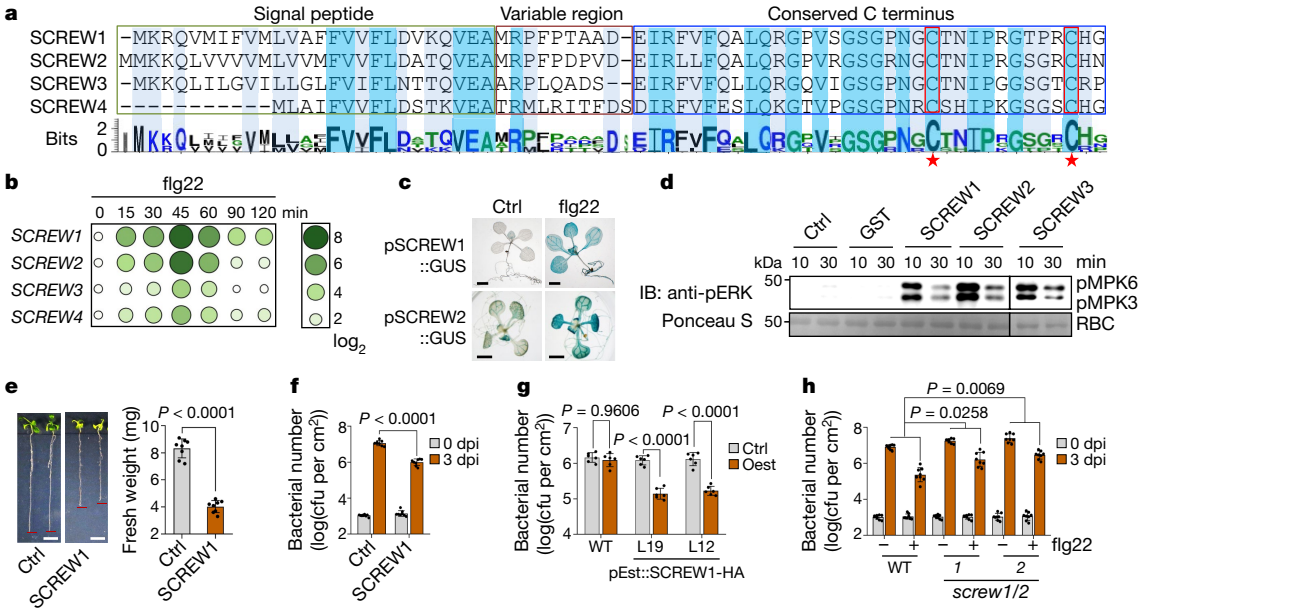

Fig. 1 | SCREWs are phytocytokines. a, Multiple sequence alignment and WebLogo analysis of SCREWs. Different domains are boxed, and conserved cysteine residues are highlighted with stars. **b**, *SCREW* genes are upregulated after flg22 treatment. Seedlings were treated with 200 nM flg22 for RT–qPCR analysis. Means ($n = 4$) of fold induction compared to non-treatment shown as $\log_2$ were used for the heat map using TBtools[45]. **c**, Flg22 upregulates the activity of *SCREW* promoters. pSCREW1/2::GUS seedlings were treated with 100 nM flg22 or ddH_2O (Ctrl) for 3 h before GUS staining. Scale bars, 2 mm. **d**, SCREWs induce MAPK activation. Seedlings were treated with protein elution buffer (Ctrl), GST or GST–SCREWs (1 μM). IB, immunoblot; RBC, Rubisco. **e**, SCREW1 inhibits seedling growth. Seedlings treated without (Ctrl) or with 1 μM SCREW1 were imaged. Fresh weights are shown as mean ± s.d. ($n = 8$). Scale bars, 1 cm. **f**, SCREW1 protects *Arabidopsis* from *Pst* DC3000 infection. Leaves were pre-infiltrated with ddH_2O (Ctrl) or 500 nM SCREW1, followed by inoculation with *Pst* DC3000. Bacterial growth was measured at 0 and 3 dpi. Data are mean ± s.d. ($n = 8$). Cfu, colony-forming units. **g**, Inducible expression of *SCREW1* enhances resistance to *Pst* DC3000. Plants carrying pEst::SCREW1-HA were spray-treated with 0.05% DMSO (Ctrl) or 50 μM β-oestradiol (Oest) for 24 h, followed by inoculation with *Pst* DC3000. Bacterial growth was measured at 3 dpi and is shown as mean ± s.d. ($n = 6$). WT, wild type. **h**, Flg22-induced resistance is partially compromised in *screw1/2* mutants. Leaves were pre-infiltrated with ddH_2O or 500 nM flg22, followed by inoculation with *Pst* DC3000. Data are mean ± s.d. ($n = 8$). Experiments were repeated at least three times with similar results. Data were analysed by two-sided Student's *t*-test (**e**, **f**) or one-way (**h**) or two-way (**g**) ANOVA followed by Tukey's test; n = biologically independent samples.

wide range of dicot and some monocot species (Extended Data Fig. 1c). Quantitative PCR with reverse transcription (RT–qPCR) analysis confirmed that *SCREW* genes were upregulated by treatment with flg22 (Fig. 1b) and treatment with elf18 (an 18-aa peptide from the bacterial elongation factor Tu (EF-Tu)), phytocytokine PLANT ELICITOR PEPTIDE 1 (Pep1) and bacterial *Pseudomonas syringae* pv. *tomato* (*Pst*) DC3000 (Extended Data Fig. 1d–f), with *SCREW1* and *SCREW2* being the most highly induced. Histochemical analysis of *GUS* expression under the control of the *SCREW1* or *SCREW2* promoter in transgenic *Arabidopsis* plants confirmed that the *SCREW* promoters were substantially induced after treatment with flg22 and primarily active in leaf veins (Fig. 1c).

To determine whether SCREWs have a role in immunity, we examined their effects on various hallmarks of PTI responses using recombinant SCREW proteins purified from *Escherichia coli* or synthetic peptides. SCREW1, SCREW2 and SCREW3 without the signal peptide, and fused with either glutathione *S*-transferase (GST) or 6×His, induced the activation of mitogen-activated protein kinases (MAPKs) (Fig. 1d, Extended Data Fig. 2a) and the expression of PTI marker genes, including *WRKY30*, *WRKY33*, *WRKY53* and *FRK1* (Extended Data Fig. 2b, c). To define the immunogenic region, we generated a series of SCREW1 truncations and synthetic peptides (Extended Data Fig. 2d). The conserved C terminus of SCREW1 without the signal peptide and variable region ($SCREW1^{39–69}$, which was used as the SCREW1 peptide hereafter) was sufficient to activate MAPKs at a subnanomolar scale (Extended Data Fig. 2d–g). Although SCREW1 induced a comparable activation of MAPKs to flg22, SCREW1 triggered a weak burst of reactive oxygen species (ROS) and a moderate increase in cytosolic calcium ($[Ca^{2+}]_{cyt}$) compared to flg22 (Extended Data Fig. 2h–j). MAMP-induced phosphorylation of the receptor-like cytoplasmic kinase (RLCK) *BOTRYTIS*-INDUCED KINASE 1 (BIK1) contributes to ROS bursts and $[Ca^{2+}]_{cyt}$ influx[18,19]. Unlike flg22, SCREW1 did not induce detectable phosphorylation of BIK1 (Extended Data Fig. 2k). Similar to flg22 and Pep1, prolonged treatment with SCREW1 inhibited seedling growth (Fig. 1e). SCREWs contain two conserved cysteine residues, which are predicted to form a disulfide bond (Fig. 1a, Extended Data Fig. 3a). Mutation of the two cysteine residues to serine in SCREW2 (SCREW2(CC/SS)) reduced its effects on MAPK activation and seedling growth inhibition (Extended Data Fig. 3b, c), indicating the importance of the conserved cysteines for the activity of SCREWs. Synthetic SCREW2 peptides with an extra step of oxidation to facilitate the formation of a disulfide bond after synthesis (SCREW2(CC)) had a similar activity to that of SCREW2 in terms of the activation of MAPKs and inhibition of the growth of *Arabidopsis* seedlings (Extended Data Fig. 3b, c), suggesting that the two cysteine residues in SCREWs might be naturally oxidized to form a disulfide bond. SCREW1 peptides do not appear to be mobile (Extended Data Fig. 3d)—similar to previous reports on Pep peptides[20]. Unlike Pep1, SCREW1 did not induce the expression of PATHOGENESIS-RELATED PROTEIN 1 (PR1) in the distal leaves with local infiltration (Extended Data Fig. 3e, f). Treatment with SCREW1 did not trigger systemic resistance to *Pst* DC3000 (Extended Data Fig. 3g). These data suggest that SCREWs might act in an autocrine or paracrine manner.

Pretreatment with SCREW1 protected *Arabidopsis* against infection with *Pst* DC3000 (Fig. 1f). In addition, oestrogen-inducible expression of C-terminal HA-tagged SCREW1 in the wild-type (WT) Col-0 background primed plant resistance against *Pst* DC3000 infection (Fig. 1g). The C-terminal HA tag did not affect the activity of SCREW1 (Extended Data Fig. 3h, i). Notably, these transgenic plants showed yellowish leaves and chlorosis, accompanied with increased *PR1* expression (Extended

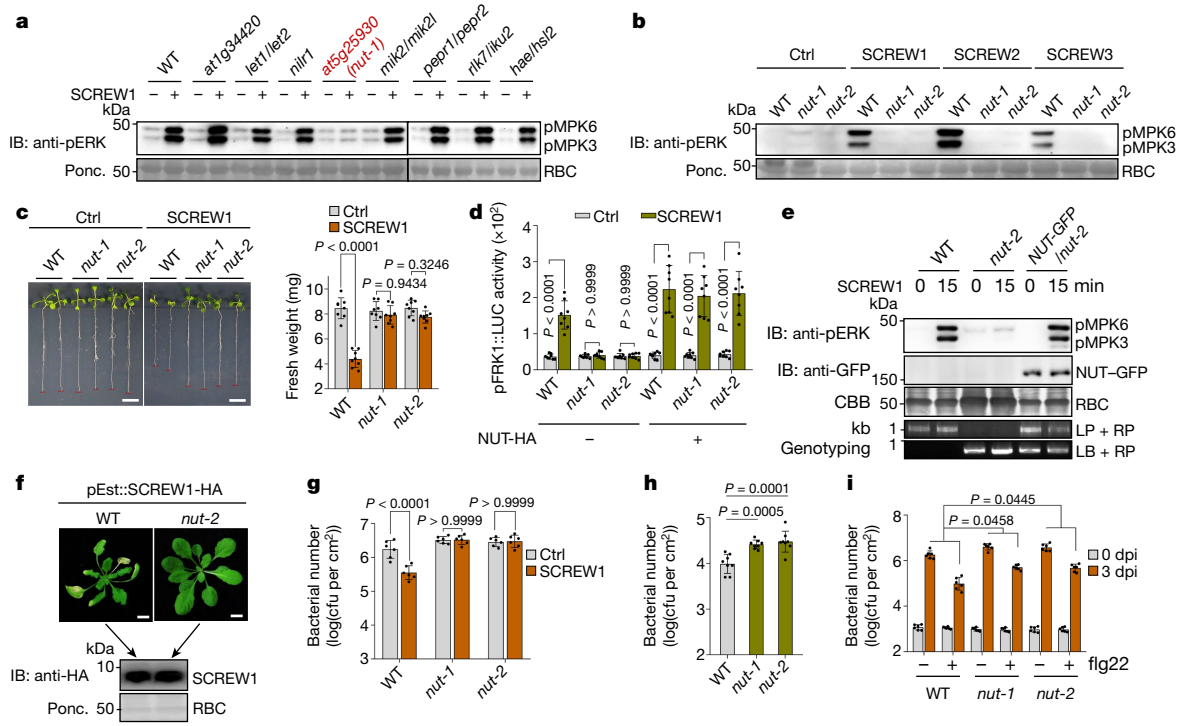

Fig. 2 | SCREWs induce NUT-dependent immune responses. a, NUT is required for SCREW1-induced MAPK activation. Plants were treated with 1 μM GST-SCREW1 for 15 min for MAPK detection. NILR1 regulates immunity to nematodes[46]. MIK2L is the homologue of MIK2. IKU2 is the homologue of RLK7. LET1 and LET2 are malectin-like receptor kinases that regulate autoimmunity[47,48]. **b**, NUT is required for MAPK activation triggered by multiple SCREWs. Plants were treated with 1 μM GST–SCREWs. **c**, NUT is required for SCREW1-induced growth inhibition. Experiments were performed as in Fig. 1e. Scale bars, 1 cm. Data are mean ± s.d. ($n = 8$). **d**, *NUT-HA* restores SCREW1-induced *FRK1* promoter activation in *nut* mutants. Protoplasts were co-transfected with pFRK1::LUC, pUBQ10::GUS, with or without p35S::NUT-HA, followed by treatment with 1 μM SCREW1. Data are shown as mean ± s.d. ($n = 8$). **e**, *NUT-GFP* restores SCREW1-induced MAPK activation in *nut-2*. Leaf discs were treated with 100 nM SCREW1 for 15 min. CBB, Coomassie brilliant blue; LP, left genomic primer; RP, right genomic primer; LB, T-DNA border primer. **f**, SCREW1-triggered leaf chlorosis is blocked in *nut-2*. Four-week-old plants were sprayed with 50 μM β-oestradiol and imaged five days later. Scale bars, 1 cm. **g**, NUT is required for SCREW1-induced resistance. Experiments were performed as in Fig. 1f. Bacterial numbers were detected at 3 dpi. Data are mean ± s.d. ($n = 6$). **h**, The *nut* mutants are more susceptible to *Pst* DC3000 *hrcC*⁻. Leaves were inoculated with *Pst* DC3000 *hrcC*⁻, and bacterial numbers were measured at 3 dpi and shown as mean ± s.d. ($n = 8$). **i**, Flg22-induced resistance is compromised in *nut* mutants. Experiments were performed as in Fig. 1h. Data are mean ± s.d. ($n = 6$). Experiments were repeated at least three times with similar results. Data were analysed by one-way (**h**, **i**) or two-way (**c**, **d**, **g**) ANOVA followed by Tukey's test; n = biologically independent samples.

Data Fig. 4a, b), after prolonged treatment with β-oestradiol at the late growth stage. Similarly, several lines of transgenic plants expressing *SCREW1* or *SCREW2* under the constitutive *35S* promoter in the wild type showed retarded growth with curled leaves, chlorosis on the old leaves and increased expression of *PR1* (Extended Data Fig. 4c, d).

As *SCREW1* and *SCREW2* were the most highly upregulated of the four *SCREW* genes after MAMP treatments (Fig. 1b), we generated *screw1/screw2* (*screw1/2*) double mutants using CRISPR–Cas9 (Extended Data Fig. 4e, f). Two homozygous mutants, *screw1/2-1* and *screw1/2-2*, showed enhanced susceptibility to *Pst* DC3000 and its type III secretion mutant *hrcC*⁻ (Extended Data Fig. 4g, h). In addition, flg22-primed resistance to *Pst* DC3000 was partially compromised in *screw1/2* mutants compared to the wild type (Fig. 1h). Our data collectively indicate that SCREWs are pathogen-inducible phytocytokines and protect plants from infection.

NUT mediates SCREW-induced immunity

Receptor kinases, especially leucine-rich repeat (LRR) receptor kinases (LRR-RKs), can function as receptors of endogenous peptides[7,8,10]. To identify the potential SCREW receptor, we screened receptor kinases with more than 18 LRRs that are induced by flg22 and for which the ligand remains unknown (Extended Data Fig. 5a). A mutant containing a T-DNA insertion in *AT5G25930*, but not others, blocked the SCREW1-triggered activation of MAPKs (Fig. 2a). AT5G25930—which we here term NUT—is an LRR-RK in the subfamily XI (Extended Data Fig. 5b). It is phylogenetically close to several LRR-RKs that are known to perceive endogenous peptides, including HAESA (HAE) and HAESA-LIKE2 (HSL2), which sense INFLORESCENCE DEFICIENT IN ABSCISSION (IDA) peptides in floral organ abscission[21], and PEP RECEPTOR 1 (PEPR1)/PEPR2 and RECEPTOR-LIKE KINASE 7 (RLK7), which sense Pep1 and PAMP-INDUCED SECRETED PEPTIDE 1 (PIP1)/PIP2, respectively[22,23] (Extended Data Fig. 5b). Similar to SCREWs, NUT is broadly conserved in dicots and monocots[24] (Extended Data Fig. 5c).

Two independent T-DNA insertion alleles of *NUT* (*nut-1* and *nut-2*) were insensitive to SCREW-triggered MAPK activation (Fig. 2b, Extended Data Fig. 5d–f), seedling growth inhibition (Fig. 2c) and *FRK1* promoter induction (Fig. 2d). Expressing *NUT* in *nut* mutant protoplasts or transgenic plants restored SCREW1-induced *FRK1* promoter induction and MAPK activation (Fig. 2d, e, Extended Data Fig. 6a). Furthermore, the inducible leaf yellowing and cell death triggered by *SCREW1* expression in wild-type plants were blocked in *nut-2* mutants (Fig. 2f, Extended Data Fig. 6b). SCREW1-induced disease resistance against *Pst* DC3000 was abolished in *nut* mutants (Fig. 2g). Similar to *screw1/2*, *nut* mutants were more susceptible to *Pst* DC3000 by either infiltration or spray inoculation (Extended Data Fig. 6c, d) and *Pst* DC3000 *hrcC*⁻ (Fig. 2h), and showed compromised flg22-induced disease resistance against *Pst* DC3000 (Fig. 2i) compared to wild-type plants. *NUT* expression was induced by treatment with different MAMPs and various pathogens,

including *Pst* DC3000, *Pst* DC3000 *avrRpm1* and the fungal pathogen *Botrytis cinerea* (Extended Data Fig. 6e), suggesting that NUT has a broad role in plant immunity. Histochemical analysis of pNUT::GUS transgenic plants implied that the *NUT* promoter was strongly induced by flg22 treatment (Extended Data Fig. 6f), similar to pSCREW1/2::GUS (Fig. 1c).

The induction of *SCREW* and *NUT* expression by different pathogens prompted us to examine whether SCREW–NUT signalling has a role in plant resistance against other pathogens and insects. The *screw* and *nut* mutants did not affect plant resistance or the hypersensitive response to *Pst* carrying the effector *avrRpm1* or *avrRpt2* (Extended Data Fig. 6g, h). However, both *screw* and *nut* mutants showed increased susceptibility to *B. cinerea* (Extended Data Fig. 6i). Moreover, the p35S::SCREW1 and p35S::SCREW2 transgenic plants were more resistant to green peach aphids (*Myzus persicae*)—a phloem-feeding insect—than wild-type plants (Extended Data Fig. 6j). Conversely, aphid reproduction was increased in the *nut* plants (Extended Data Fig. 6k), indicating that SCREW–NUT has a role in the resistance of plants to aphids. Moreover, aphid feeding induced the expression of *SCREW* and *NUT* genes, as well as the activity of pNUT::GUS (Extended Data Fig. 6l, m). This insect infests plants through its specialized mouthpart that penetrates plant tissues and sucks saps from the phloem[25]. This is consistent with the observation of increased expression of pSCREW::GUS and pNUT::GUS in vascular tissues (Fig. 1c, Extended Data Fig. 6f). Together, the data show that SCREW–NUT has a vital role in plant resistance against various pests, including bacterial *P. syringe*, fungal *B. cinerea*, and sap-feeding green peach aphids.

NUT is the receptor of SCREWs

NUT consists of an extracellular domain of 22 LRRs, a transmembrane domain and a cytoplasmic kinase domain (Fig. 3a). NUT–GFP is primarily localized at the plasma membrane in *Arabidopsis* transgenic plants and *Nicotiana benthamiana* (Extended Data Fig. 7a, b). Treatment with SCREW1 induced NUT endocytosis (Fig. 3b). The NUT kinase domain is annotated as an arginine–aspartate (RD) kinase (Extended Data Fig. 7c). The GST-tagged NUT cytosolic domain (NUT_{CD})—but not its kinase-inactive mutant NUT_{CD}(K714E), which contains a Lys-to-Glu mutation in the ATP-binding site—possessed an autophosphorylation activity (Fig. 3c, Extended Data Fig. 7c), implying that NUT is a functional kinase. Unlike NUT, NUT(K714E) did not restore the SCREW1-triggered activation of MAPKs in *nut-1* (Fig. 3d), supporting the functional importance of the NUT kinase activity.

When immunoprecipitated from plant cells, NUT—but not FLS2, the LRR-RK receptor of flg22—pulled down biotinylated SCREW1 (Fig. 3e). Excessive non-labelled SCREW1, and not flg22, competed for biotin–SCREW1 binding to NUT (Fig. 3e), indicating a specific interaction between SCREW1 and NUT. Surface plasmon resonance (SPR) assays with the NUT extracellular domain (NUT_{ECD}) purified from insect cells showed that NUT_{ECD} bound to SCREW1 with a dissociation constant (K_d) of 12.97 μM and SCREW2 with a K_d of 6.23 μM at pH 7.5 (Fig. 3f, g). NUT_{ECD} also bound to SCREW1, SCREW2 and SCREW1–HA at pH 5.7, similar to the apoplastic pH under the normal growth condition (Extended Data Fig. 7d–f). The two conserved cysteine residues are essential for the binding of SCREW2 to NUT_{ECD} (Extended Data Fig. 7g). Moreover, SCREW2(ΔC8), a deletion variant without the C-terminal eight amino acids, showed a substantial reduction in binding affinity to NUT and could no longer activate MAPKs and inhibit seedling growth compared to SCREW2 (Extended Data Figs. 3b, c, 7h). Together, the data indicate that NUT binds to SCREW1 and SCREW2 in vivo and in vitro, and that NUT is the receptor of SCREW1 and SCREW2.

SCREW–NUT functions through SERKs

BRASSINOSTEROID INSENSITIVE 1-ASSOCIATED RECEPTOR KINASE 1 (BAK1) and its related SERKs are co-receptors of multiple LRR-RKs[26]. SCREW1 and SCREW2 stimulated the formation of complexes of NUT and BAK1 (Fig. 3h). SPR assays indicated that BAK1 markedly increased the binding between NUT_{ECD} and SCREW2, with a K_d of 0.38 μM (Extended Data Fig. 7i). SCREW1-induced seedling growth inhibition was abolished in the *bak1-5/serk4-1* mutant (Fig. 3i). Moreover, SCREW1-mediated resistance against *Pst* DC3000 was compromised in *bak1-5/serk4-1* (Fig. 3j).

RLCK BIK1 associates with multiple PRRs and relays downstream signalling events[18,27]. Notably, we did not detect an interaction of BIK1 with NUT, although BIK1 formed a complex with PEPR1 (Extended Data Fig. 7j). BIK1 was also not required for the SCREW1-induced inhibition of seedling growth (Extended Data Fig. 7k). In line with the observations that SCREW1 did not induce detectable BIK1 phosphorylation and weakly activated ROS burst (Extended Data Fig. 2i, k), SCREW–NUT might activate a BIK1-independent signalling pathway. Alternatively, other RLCKs might function redundantly with BIK1 in relaying the SCREW–NUT signalling.

SCREW–NUT reopens stomata in immunity

Phyllosphere microorganisms exploit stomata as entry points to invade the leaf apoplasts, which are an aqueous habitat for microbial colonization[4]. As a defence mechanism, MAMPs and DAMPs induce stomatal closure to prevent pathogen entry[28]. In contrast to flg22, treatment with SCREW1 did not induce stomatal closure in wild-type plants (Extended Data Fig. 8a). Of note, SCREW1 suppressed flg22-induced stomatal closure (Fig. 4a, Extended Data Fig. 8a). SCREW–NUT did not affect the flg22-induced formation of the FLS2–BAK1 complex or MAPK activation, suggesting that SCREW does not affect the activity of flg22 per se (Extended Data Fig. 8b–d). SCREW1-mediated suppression of flg22-induced stomatal closure was abolished in *nut* mutants (Fig. 4a). Thus, the SCREW1–NUT signalling counteracts flg22-induced stomatal closure. Furthermore, we observed a gradual reopening of stomata at three and four hours after flg22 treatment in wild-type plants, which was compromised in *nut* and *screw1/2* mutants (Fig. 4b). These data suggest that SCREW–NUT might mediate the subsequent reopening of stomata, which are initially closed upon the perception of MAMPs during pathogen invasions.

Water availability in apoplasts is a crucial determinant for pathogen colonization[29,30]. After sensing MAMPs, plants close their stomata to restrict pathogen entry. Inevitably, closed stomata prevent water loss in apoplasts and create living niches for bacterial colonization. How plants counteract the detrimental effects that are caused by the prolonged stomatal closure remains unclear. We monitored the stomatal conductance—a quantitative measurement of stomatal opening—during infections. As reported, after infection with *Pst* DC3000, the stomatal conductance was initially decreased and then gradually increased in wild-type plants[31] (Fig. 4c). The increased stomatal conductance was compromised in *screw1/2* and *nut* mutants (Fig. 4c), reinforcing that SCREW–NUT mediates stomatal reopening during pathogen invasions. Thus, SCREW–NUT might function as a defence mechanism to subsequently reopen the stomata, which were closed upon MAMP perception, and promote water loss, thereby disrupting an aqueous habitat for pathogen colonization. The vesicle-trafficking-related HOPM INTERACTOR 7 (MIN7) regulates the aqueous apoplasts[32]. Notably, the *min7* mutant was partially compromised in SCREW1-induced resistance to *Pst* DC3000, but did not affect SCREW1-induced MAPK activation and growth inhibition (Extended Data Fig. 8e–g), suggesting that SCREW–NUT might function partially overlapping with MIN7 downstream or independently of MAPK activation and growth inhibition.

To test whether SCREW–NUT-mediated stomatal reopening leads to a water potential change in apoplasts, we used a water-potential-responding reporter, pProU::GFP, in which *GFP* is under the promoter of the *E. coli ProU* operon, rapidly activated by the reduced water potential and thus used as a whole-cell biosensor for water availability[33]. *Pst* DC3000 containing pNptII::GFP, the expression of which is

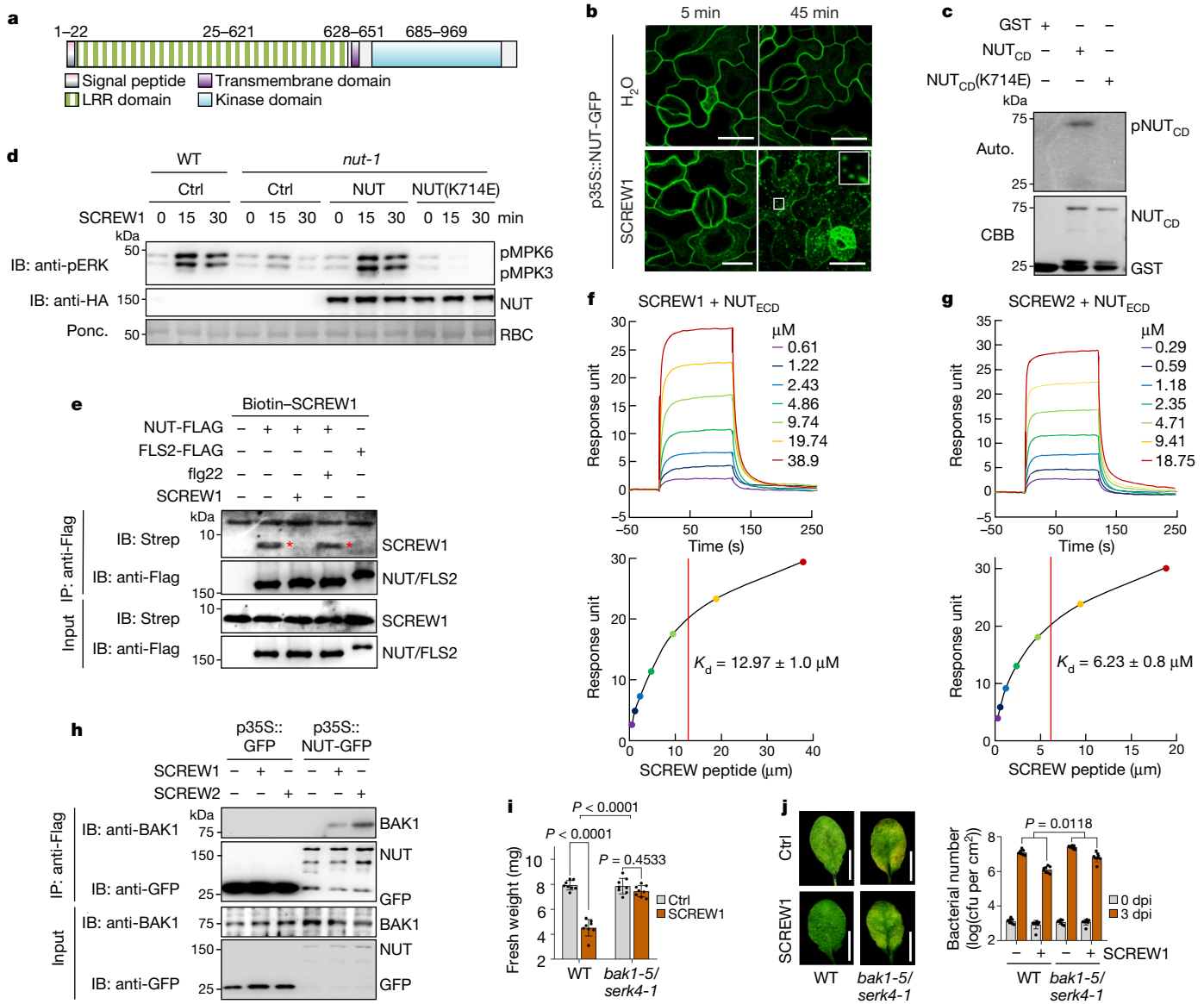

Fig. 3 | NUT is the SCREW receptor. a, Diagram of NUT protein domains with amino acid positions labelled. **b**, SCREW1 induces NUT–GFP endocytosis. Seedlings treated with H_2O or 100 nM SCREW1 were imaged using confocal microscopy. Insert is a 3× magnification. Scale bars, 20 μm. **c**, NUT exhibits autophosphorylation activity. Phosphorylation is shown by autoradiogram. **d**, NUT(K714E) does not restore SCREW1-induced MAPK activation in *nut-1*. Protoplasts expressing NUT–HA or NUT(K714E)–HA were treated with 100 nM SCREW1. **e**, SCREW1 binds to plant-expressed NUT. NUT–Flag or FLS2–Flag expressed in protoplasts were incubated with 100 nM biotin–SCREW1 for an immunoprecipitation (IP) assay, and non-labelled SCREW1 or flg22 (10 μM) was used as a competitor. **f**, SCREW1 binds to NUT_{ECD} in SPR assays. Top, SPR sensorgram profile of SCREW1 peptides at gradient concentrations on a sensor chip immobilized with NUT_{ECD}. Bottom, steady-state affinity (binding at equilibrium). **g**, SCREW2 binds to NUT_{ECD} in SPR assays. SPR assays (**f**, **g**) were performed at pH 7.5. **h**, SCREWs induce NUT and BAK1 association in plants. Seedlings were treated with 1 μM SCREW for 30 min. NUT–BAK1 association was detected with co-immunoprecipitation using anti-BAK1 or anti-GFP antibodies. **i**, *bak1-5/serk4-1* is insensitive to SCREW1-induced growth inhibition. Experiments were performed as in Fig. 1e. Data are mean ± s.d. ($n = 8$). **j**, *bak1-5/serk4-1* is compromised in SCREW1-induced resistance to *Pst* DC3000. Experiments were performed as in Fig. 1f. Disease symptoms were observed at 3 dpi. Scale bars, 1 cm. Data are mean ± s.d. ($n = 8$). Experiments were repeated three (**b**–**e**, **h**–**j**) or two (**f**, **g**) times with similar results. Data were analysed by two-sided Student's *t*-test (**i**, j) and two-way ANOVA followed by Tukey's test (**i**); *n* = biologically independent samples.

driven by the constitutive neomycin phosphotransferase gene promoter and not affected by water potential, was included as a control for bacterial growth. The expression of pNptII::GFP was gradually increased at 6 and 9 hours post-infection (hpi) (Fig. 4d), indicating in planta bacterial multiplication. The expression of pNptII::GFP in *nut* was higher than that in the wild type at 9 hpi (Fig. 4d), corroborating the increased susceptibility of *nut* to *Pst* DC3000 (Extended Data Fig. 6c, d). Notably, the expression of pProU::GFP in *nut* was lower than that in the wild type at 9 hpi (Fig. 4d). Quantification of the expression of pProU::GFP relative to pNptII::GFP from three independent repeats indicated statistically significant differences between wild-type and *nut* mutant plants at 9 hpi (Fig. 4e). The data indicate that water potential in *nut* mutants is higher than in wild-type plants after infection with *Pst* DC3000, implying that SCREW–NUT negatively regulates the water potential during infection. High humidity promotes bacterial multiplication and the water-soaking disease phenotype by maintaining aqueous apoplasts during infection[32]. Under increased humidity (85–98%) with transient apoplast water supplementation[32], the increased susceptibility and bacterial multiplication

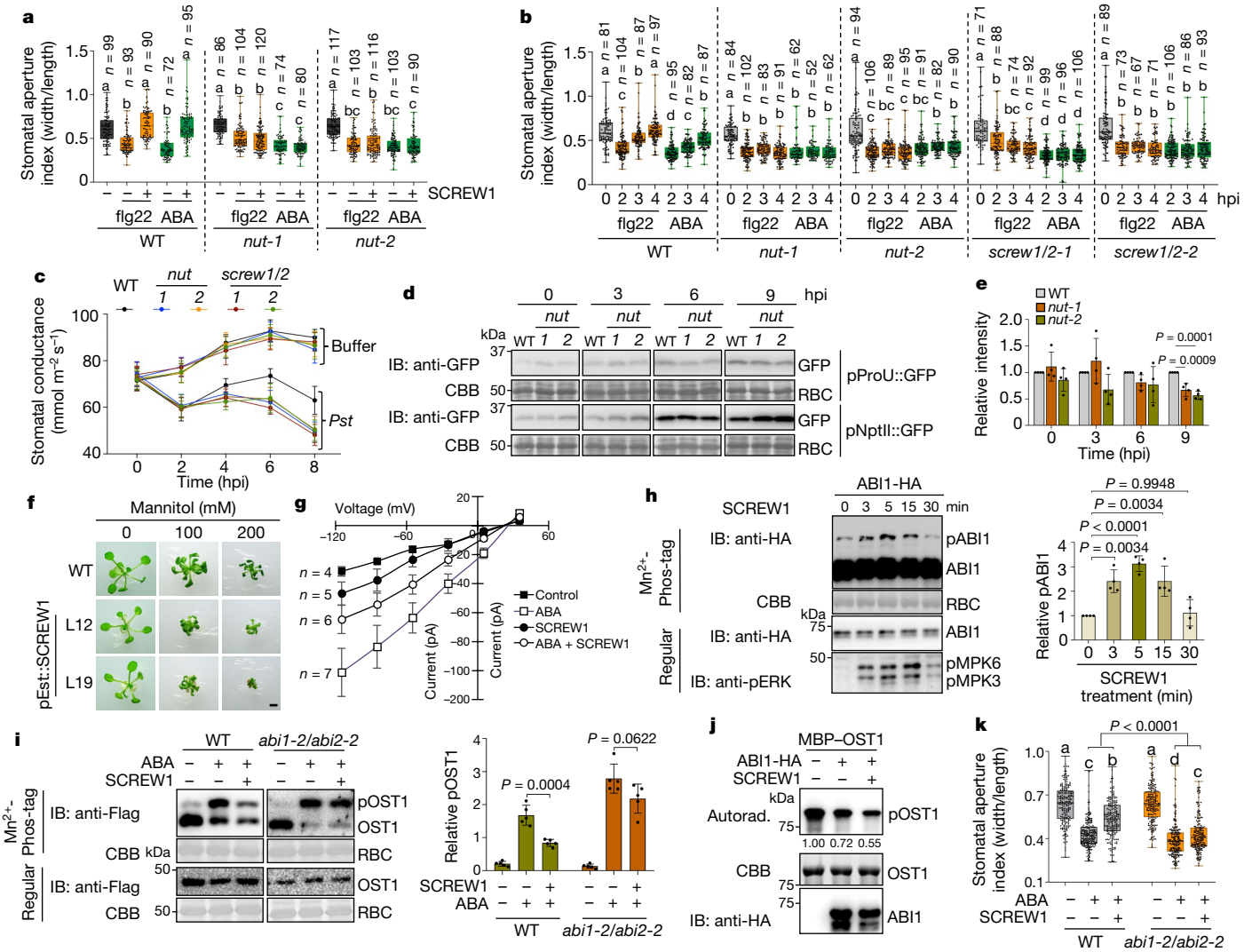

Fig. 4 | SCREW–NUT counter-regulates ABA- and MAMP-induced stomatal closure. a, SCREW1 suppresses NUT-dependent flg22- and ABA-induced stomatal closure. Stomatal apertures were measured after treatment with flg22, ABA or in combination with SCREW1 for 2 h. **b**, *screw1/2* and *nut* are compromised in reopening stomata. **c**, Reduced stomatal conductance in *nut* and *screw1/2* mutants after infection. Leaves were inoculated with $MgCl_2$ (buffer) or *Pst* DC3000 ($n = 12$). **d**, Increased water potential in *nut* after infection. Leaves were infiltrated with *Pst* DC3000 carrying pProU::GFP or pNptII::GFP. **e**, Quantification of GFP expression in **d** ($n = 4$). **f**, Enhanced sensitivity to mannitol treatment of pEst::SCREW1-HA plants. Scale bar, 2 mm. **g**, SCREW1 reduces ABA activation of S-type anion channels. **h**, SCREW1 induces ABI1 phosphorylation. Protoplasts expressing ABI1–HA were treated with 1 μM SCREW1. Proteins were separated with Mn^{2+}-Phos-tag or regular SDS–PAGE ($n = 4$). **i**, SCREW1 suppresses ABA-induced OST1 phosphorylation in an ABI-dependent manner. Protoplasts expressing OST1–Flag were treated with SCREW1 for 5 min and then ABA for 5 min ($n = 5$). **j**, SCREW1 increases ABI1 phosphatase activity towards OST1. ABI1–HA proteins immunoprecipitated from protoplasts treated with and without SCREW1 were used for a kinase assay. Averages of three independent repeats are labelled. **k**, ABI1 and ABI2 are required for SCREW1 suppression on ABA-induced stomatal closure ($n = 202$). Experiments were repeated at least three times with similar results. Data are shown as box plots as defined in the Methods (**a**, **b**, **k**), mean ± s.d. (**c**, **e**, **h**, **i**), or mean ± s.e.m. (**g**). Data were analysed by one-way (**a**, **b**, **e**, **h**) or two-way (**k**) ANOVA followed by Tukey's test, or two-sided Student's *t*-test (**g**, **i**, **k**). Different letters (**a**, **b**, **k**) denote a statistically significant difference ($P < 0.05$). Statistical analysis was performed within the same genotype (**a**, **b**). *n* = biologically independent samples.

in *screw1/2* or *nut* mutants became less apparent (Extended Data Fig. 8h). In addition, SCREW1 no longer induced plant resistance to *Pst* DC3000 under high humidity with transient apoplast water supplementation (Extended Data Fig. 8i). Together, our studies reveal the critical role of SCREW–NUT in plant immunity through modulating stomatal reopening and the apoplastic water level.

SCREW–NUT modulates plant water loss

Plants expressing p35S::SCREW1 or p35S::SCREW2 showed leaf wilting and curling, partially resembling plants under dehydration (Extended Data Fig. 9a). These transgenic plants also exhibited increased water loss in response to dehydration compared to wild-type plants (Extended Data Fig. 9b). In addition, inducible expression of *SCREW1* rendered plants more sensitive to mannitol—a causative agent of the drought osmotic stress—than wild-type plants (Fig. 4f).

Conversely, *screw1/2* and *nut* mutants exhibited reduced water loss and sensitivity to mannitol treatment compared to wild-type plants (Extended Data Fig. 9c, d). Notably, *screw1/2* and *nut* mutants had the normal permeability and thickness of plant cuticle—one of the barriers protecting plants from water loss—as indicated by toluidine blue staining[34] or transmission electron microscopy analysis (Extended Data Fig. 9e–g). The plant hormone ABA mediates plant water usage and drought tolerance[35,36]. Consistent with the reduced water loss,

screw1/2 and *nut* mutants were more sensitive to ABA treatment than wild-type plants (Extended Data Fig. 9h). Under water-deficit stress, the increased levels of ABA promote stomatal closure to prevent water loss[3]. ABA-induced stomatal closure was suppressed by treatment with SCREW1 (Extended Data Fig. 8a). In addition, SCREW1 and SCREW2 suppressed the ABA-induced expression of the desiccation-responsive genes *RESPONSIVE TO ABA 18* (*RAB18*) and *RESPONSIVE TO DESICCATION 29A* (*RD29A*) (Extended Data Fig. 9i). The SCREW1-mediated suppression of ABA-induced stomatal closure depended on NUT (Fig. 4a). Like flg22 treatment, the gradual reopening of ABA-induced stomatal closure depended on SCREW–NUT signalling (Fig. 4b). Moreover, *SCREW* and *NUT* transcripts were upregulated by ABA treatment, drought and mannitol treatment (Extended Data Fig. 9j, k). Thus, the data suggest that SCREW–NUT has a critical role in modulating plant water loss by antagonizing ABA-induced stomatal closure.

SCREW–NUT regulates the ABI–OST1 module

Stomatal aperture is mainly controlled by a core signalling module that consists of type 2C protein phosphatases (PP2Cs), including ABI1 and ABI2, and SNF1-related protein kinases (SnRK2s), most importantly OST1 (SnRK2.6), which regulates S-type anion channels such as SLOW ANION CHANNEL-ASSOCIATED 1 (SLAC1) to drive plasma membrane depolarization and subsequent K^+ efflux[2,37]. The activation of S-type anion channels is a critical step in stomatal closure[38,39]. Whole-cell recordings of anion channel currents in wild-type guard cells indicated that SCREW1 suppressed the ABA-induced activation of S-type anion channels (Fig. 4g). Of note, treatment with SCREW1 induced the phosphorylation of ABI1 and ABI2, but not OST1, as revealed by Phos-tag immunoblotting (Fig. 4h, Extended Data Fig. 10a, b). Furthermore, the SCREW1-induced ABI1 phosphorylation was no longer observed in *nut-2*, and expression of NUT–Flag restored ABI1 phosphorylation (Extended Data Fig. 10c).

ABA treatment induces the phosphorylation of OST1, a critical kinase in regulating stomatal closure[6,40] (Extended Data Fig. 11a, b). Expression of ABI1 or ABI2 blocked ABA-induced OST1 phosphorylation (Extended Data Fig. 11a, b), consistent with ABI phosphatase-mediated dephosphorylation and inhibition of OST1[2,37]. Treatment with SCREW1 suppressed ABA-induced OST1 phosphorylation in a dosage-dependent manner (Fig. 4i, Extended Data Fig. 11c). We further tested whether ABI1 phosphorylation by SCREW–NUT could enhance its phosphatase activity. ABI1–HA immunoprecipitated from plant cells dephosphorylated purified MBP-tagged OST1 proteins (Fig. 4j). In addition, ABI1 stimulated with SCREW1 treatment exhibited an enhanced phosphatase activity towards OST1 (Fig. 4j). ABI1–HA co-immunoprecipitated with NUT–Flag in plant cells (Extended Data Fig. 11d). His-tagged ABI1 directly interacted with GST-tagged NUT_{CD} (Extended Data Fig. 11e). Together, the data indicate that SCREW–NUT regulates ABI phosphorylation and enhances its phosphatase activity, thereby reducing OST1 phosphorylation and the activity of S-type anion channels.

As SCREW–NUT targets ABIs, which dephosphorylate OST1, we tested the requirement of ABI1 and ABI2 for SCREW-regulated OST1 phosphorylation and stomatal opening. The SCREW1-triggered suppression of ABA-induced OST1 phosphorylation was compromised in the loss-of-function *abi1-2/abi2-2* mutant (Fig. 4i). The SCREW1-mediated suppression of ABA-induced stomatal closure was also reduced in *abi1-2/abi2-2* (Fig. 4k). In addition, ABI1 and ABI2 are partially required for the SCREW1-mediated suppression of flg22-induced stomatal closure (Extended Data Fig. 12a). Thus, our biochemical and genetic data indicate that SCREW–NUT regulates the stomatal aperture through the ABI–OST1 phosphorylation module.

Discussion

Terrestrial plants rely on stomata to facilitate gas exchange and water vapour between plants and the environment[1,2]. Under water-deficit stress, leaf cells sense changes in water potential and accumulate ABA, which leads to stomatal closure and decreased transpiration to prevent water loss[3,36]. As a defence strategy, plants close their stomata after sensing infections to limit the entry of pathogens, including bacteria and fungi[28,41]. However, stomatal closure prevents the uptake of CO_2 and reduces transpiration and photosynthesis. Meanwhile, stomatal closure restricts water loss and leads to a rapid increase in apoplastic water content, favouring bacterial colonization[29,30]. Thus, long-term stomatal closure is detrimental to plants, and plants must have evolved a mechanism to enable this process to be transient at the whole-plant level. Stomata also emerge as important mediators of plant–herbivore interactions[42]. We report here that a peptide–receptor pair, which is induced after pathogen exposure and dehydration, reopens the stomata and acts in concert with MAMP- and ABA-induced stomatal closure to enable stomatal movement to be a dynamic process in the plant response to pathogen and insect attacks and water deficiency.

Without infections, *SCREW*s and *NUT* are weakly expressed. The SCREW–NUT signalling may not be active at the initial pathogen invasion stage. After a MAMP is perceived, the expression of *SCREW*s and *NUT* is markedly increased. MAMP-PRR signalling induces SCREW–NUT to reopen the stomata, consequently disrupting the microorganism-rich aqueous habitat and suppressing the proliferation of pathogens at the post-invasion stage (Extended Data Fig. 12b). SCREW–NUT also counter-regulates ABA-induced stomatal closure and promotes water loss in response to dehydration, consistent with a previous report about the role of NUT (also named HAESA-LIKE3, HSL3) in stomatal closure and drought stress[43]. A recent preprint also reports that HSL3 is the receptor for SCREWs (named CTNIPs there)[44]. Cross-talk between ABA- and MAMP-induced stomatal closure has been observed[5]. OST1 is a crucial kinase that functions downstream of ABIs in ABA- and flg22-induced stomatal closure[5,6]. We show here that SCREW–NUT induces ABI phosphorylation and enhances ABI phosphatase activity, thereby reducing OST1 phosphorylation and the activation of S-type anion channels. Thus, SCREW–NUT regulates the stomatal aperture by targeting the ABI-OST1 signalling module.

In summary, the SCREW–NUT peptide–receptor pair modulates two different facets of plant physiology in response to attacks by pathogens and dehydration by controlling stomatal reopening. SCREW–NUT homologues are broadly conserved in dicots and monocots. The SCREW–NUT-regulated stomatal movement dynamics are likely to be a widespread mechanism to ensure a balanced physiological response at the whole-plant level in response to biotic and abiotic stresses.

Online content

Any methods, additional references, Nature Research reporting summaries, source data, extended data, supplementary information, acknowledgements, peer review information; details of author contributions and competing interests; and statements of data and code availability are available at https://doi.org/10.1038/s41586-022-04684-3.

1. Hetherington, A. M. & Woodward, F. I. The role of stomata in sensing and driving environmental change. *Nature* **424**, 901–908 (2003).
2. Sussmilch, F. C., Schultz, J., Hedrich, R. & Roelfsema, M. R. G. Acquiring control: the evolution of stomatal signalling pathways. *Trends Plant Sci.* **24**, 342–351 (2019).
3. Hsu, P. K., Dubeaux, G., Takahashi, Y. & Schroeder, J. I. Signaling mechanisms in abscisic acid-mediated stomatal closure. *Plant J.* **2**, 307–321 (2021).
4. Melotto, M., Underwood, W. & He, S. Y. Role of stomata in plant innate immunity and foliar bacterial diseases. *Annu. Rev. Phytopathol.* **46**, 101–122 (2008).
5. Guzel Deger, A. et al. Guard cell SLAC1-type anion channels mediate flagellin-induced stomatal closure. *New Phytol.* **208**, 162–173 (2015).
6. Mustilli, A. C., Merlot, S., Vavasseur, A., Fenzi, F. & Giraudat, J. Arabidopsis OST1 protein kinase mediates the regulation of stomatal aperture by abscisic acid and acts upstream of reactive oxygen species production. *Plant Cell* **14**, 3089–3099 (2002).
7. Takahashi, F., Hanada, K., Kondo, T. & Shinozaki, K. Hormone-like peptides and small coding genes in plant stress signaling and development. *Curr. Opin. Plant Biol.* **51**, 88–95 (2019).
8. Olsson, V. et al. Look closely, the beautiful may be small: precursor-derived peptides in plants. *Annu. Rev. Plant Biol.* **70**, 153–186 (2019).

9. Tang, D., Wang, G. & Zhou, J. M. Receptor kinases in plant–pathogen interactions: more than pattern recognition. *Plant Cell* **29**, 618–637 (2017).
10. Dievart, A., Gottin, C., Perin, C., Ranwez, V. & Chantret, N. Origin and diversity of plant receptor-like kinases. *Annu. Rev. Plant Biol.* **71**, 131–156 (2020).
11. Couto, D. & Zipfel, C. Regulation of pattern recognition receptor signalling in plants. *Nat. Rev. Immunol.* **16**, 537–552 (2016).
12. Zhou, J. M. & Zhang, Y. Plant immunity: danger perception and signaling. *Cell* **181**, 978–989 (2020).
13. Hou, S., Liu, D. & He, P. Phytocytokines function as immunological modulators of plant immunity. *Stress Biol.* **1**, 8 (2021).
14. Tanaka, K. & Heil, M. Damage-associated molecular patterns (DAMPs) in plant innate immunity: applying the danger model and evolutionary perspectives. *Annu. Rev. Phytopathol.* **59**, 53–75 (2021).
15. Hou, S. et al. The Arabidopsis MIK2 receptor elicits immunity by sensing a conserved signature from phytocytokines and microbes. *Nat. Commun.* **12**, 5494 (2021).
16. Rhodes, J. et al. Perception of a divergent family of phytocytokines by the Arabidopsis receptor kinase MIK2. *Nat. Commun.* **12**, 705 (2021).
17. Li, F. et al. Modulation of RNA polymerase II phosphorylation downstream of pathogen perception orchestrates plant immunity. *Cell Host Microbe* **16**, 748–758 (2014).
18. Liang, X. & Zhou, J. M. Receptor-like cytoplasmic kinases: central players in plant receptor kinase-mediated signaling. *Annu. Rev. Plant Biol.* **69**, 267–299 (2018).
19. Xu, G., Moeder, W., Yoshioka, K. & Shan, L. A tale of many families: calcium channels in plant immunity. *Plant Cell* **2022**, koac033 (2022).
20. Ross, A. et al. The *Arabidopsis* PEPR pathway couples local and systemic plant immunity. *EMBO J.* **33**, 62–75 (2014).
21. Santiago, J. et al. Mechanistic insight into a peptide hormone signaling complex mediating floral organ abscission. *eLife* **5**, e15075 (2016).
22. Yamaguchi, Y., Huffaker, A., Bryan, A. C., Tax, F. E. & Ryan, C. A. PEPR2 is a second receptor for the Pep1 and Pep2 peptides and contributes to defense responses in *Arabidopsis*. *Plant Cell* **22**, 508–522 (2010).
23. Hou, S. et al. The secreted peptide PIP1 amplifies immunity through receptor-like kinase 7. *PLoS Pathog.* **10**, e1004331 (2014).
24. Furumizu, C. et al. The sequenced genomes of nonflowering land plants reveal the innovative evolutionary history of peptide signaling. *Plant Cell* **33**, 2915–2934 (2021).
25. Chen, Y. et al. An aphid RNA transcript migrates systemically within plants and is a virulence factor. *Proc. Natl Acad. Sci. USA* **117**, 12763–12771 (2020).
26. Ma, X., Xu, G., He, P. & Shan, L. SERKing coreceptors for receptors. *Trends Plant Sci.* **21**, 1017–1033 (2016).
27. Lin, W., Ma, X., Shan, L. & He, P. Big roles of small kinases: the complex functions of receptor-like cytoplasmic kinases in plant immunity and development. *J. Integr. Plant Biol.* **55**, 1188–1197 (2013).
28. Melotto, M., Underwood, W., Koczan, J., Nomura, K. & He, S. Y. Plant stomata function in innate immunity against bacterial invasion. *Cell* **126**, 969–980 (2006).
29. Aung, K., Jiang, Y. & He, S. Y. The role of water in plant–microbe interactions. *Plant J.* **93**, 771–780 (2018).
30. Beattie, G. A. Water relations in the interaction of foliar bacterial pathogens with plants. *Annu. Rev. Phytopathol.* **49**, 533–555 (2011).
31. Freeman, B. C. & Beattie, G. A. Bacterial growth restriction during host resistance to *Pseudomonas syringae* is associated with leaf water loss and localized cessation of vascular activity in *Arabidopsis thaliana*. *Mol. Plant Microbe Interact.* **22**, 857–867 (2009).
32. Xin, X. F. et al. Bacteria establish an aqueous living space in plants crucial for virulence. *Nature* **539**, 524–529 (2016).
33. Axtell, C. A. & Beattie, G. A. Construction and characterization of a proU-gfp transcriptional fusion that measures water availability in a microbial habitat. *Appl. Environ. Microbiol.* **68**, 4604–4612 (2002).
34. Tanaka, T., Tanaka, H., Machida, C., Watanabe, M. & Machida, Y. A new method for rapid visualization of defects in leaf cuticle reveals five intrinsic patterns of surface defects in Arabidopsis. *Plant J.* **37**, 139–146 (2004).
35. Yoshida, T., Mogami, J. & Yamaguchi-Shinozaki, K. ABA-dependent and ABA-independent signaling in response to osmotic stress in plants. *Curr. Opin. Plant Biol.* **21**, 133–139 (2014).
36. Zhu, J. K. Abiotic stress signaling and responses in plants. *Cell* **167**, 313–324 (2016).
37. Munemasa, S. et al. Mechanisms of abscisic acid-mediated control of stomatal aperture. *Curr. Opin. Plant Biol.* **28**, 154–162 (2015).
38. Vahisalu, T. et al. SLAC1 is required for plant guard cell S-type anion channel function in stomatal signalling. *Nature* **452**, 487–U415 (2008).
39. Maierhofer, T. et al. Site- and kinase-specific phosphorylation-mediated activation of SLAC1, a guard cell anion channel stimulated by abscisic acid. *Sci. Signal.* **7**, ra86 (2014).
40. Yoshida, R. et al. ABA-activated SnRK2 protein kinase is required for dehydration stress signaling in *Arabidopsis*. *Plant Cell Physiol.* **43**, 1473–1483 (2002).
41. Ye, W. et al. Stomatal immunity against fungal invasion comprises not only chitin-induced stomatal closure but also chitosan-induced guard cell death. *Proc. Natl Acad. Sci. USA* **117**, 20932–20942 (2020).
42. Lin, P. A. et al. Stomata-mediated interactions between plants, herbivores, and the environment. Trends Plant Sci. (2021).
43. Liu, X. S. et al. The LRR-RLK protein HSL3 regulates stomatal closure and the drought stress response by modulating hydrogen peroxide homeostasis. *Front. Plant Sci.* **11**, 548034 (2020).
44. Rhodes, J. et al. Perception of a conserved family of plant signalling peptides by the receptor kinase HSL3. Preprint at *bioRxiv* https://doi.org/10.1101/2021.10.25.465685 (2022).
45. Wu, F. et al. Hydrogen peroxide sensor HPCA1 is an LRR receptor kinase in *Arabidopsis*. *Nature* **578**, 577–581 (2020).
46. Mendy, B. et al. *Arabidopsis* leucine-rich repeat receptor–like kinase NILR1 is required for induction of innate immunity to parasitic nematodes. *PLoS Pathog.* **13**, e1006284 (2017).
47. Huang, Y. et al. A trimeric CrRLK1L–LLG1 complex genetically modulates SUMM2-mediated autoimmunity. *Nat. Commun.* **11**, 4859 (2020).
48. Liu, J. et al. The malectin-like receptor-like kinase LETUM1 modulates NLR protein SUMM2 activation via MEKK2 scaffolding. *Nat. Plants* **6**, 1106–1115 (2020).

Methods

Plant materials and growth conditions

The *Arabidopsis thaliana* accession Columbia-0 (Col-0) was used as the wild type. T-DNA insertion mutants *nut-1* (WiscDsLox450B04), *mik2-1* (SALK_061769), *mik2-like* (SALK_112341) and *nilr1* (SAIL_859-H01) were obtained from the Nottingham *Arabidopsis* Stock Centre (NASC), and *nut-2* (SALK_207895) and *at1g34420* (SALK_033924C) were from the *Arabidopsis* Biological Resource Center (ABRC). The *fls2*, *bak1-3*, *bak1-4*, *bak1-5*, *sobir1-12*, *bik1*, *bak1-5/serk4-1*, *hae/hsl2*, *pepr1-2/pepr2-2*, *rlk7-2/iku2-1*, *mik2-1/mik2-l*, *let1/let2*, *min7* and *abi1-2/abi2-2* mutants were reported in previous studies[15,23,32,47,49–52]. The double mutants were generated by genetic crossing. The pNUT::GUS seeds were from J. Li[53]. All *Arabidopsis* plants, unless otherwise stated, were grown on soil (Metro Mix 366, Sunshine LP5 or Sunshine LC1, Jolly Gardener C/20 or C/GP) in a growth room at 20–23 °C, 50% humidity and 100 μE m^{-2} s^{-2} light with a 12-h light–12-h dark photoperiod. Four- to five-week-old plants were used for protoplast isolation, disease assays and detection of ROS production, callose deposition and stomatal movement. Seedlings used for analyses of growth inhibition, MAPK activation, gene transcription and β-glucuronidase (GUS) staining were grown on half-strength Murashige and Skoog ($^1/_2$MS) plates containing 0.5% (w/v) sucrose and 0.75% (w/v) agar, pH 5.7, under the same growth conditions as plants grown on soil. Tobacco (*Nicotiana benthamiana*) was grown on Sunshine LP5 soil under a 14-h light/10-h dark photoperiod at 23 °C.

Plasmid construction, protoplast transfection and *Arabidopsis* transformation

pFRK1::LUC, pUBQ10::GUS, pHBT-35S::SERK-HA, pHBT-35S::FLS2-Flag, and pHBT-35S::FLS2-GFP and pHBT-35S::PEPR1-Flag were described previously[49,54]. *SCREW1* and *SCREW2* were PCR-amplified from Col-0 cDNA using gene-specific primers with BamHI at the 5′ end and StuI or SmaI at the 3′ end, followed by digestion with BamHI and StuI or SmaI and ligation into the *pHBT* vector with the HA sequence at the 3′ end to generate pHBT-35S::SCREW1, 2-HA. *NUT* was amplified from Col-0 genomic DNAs using gene-specific primers with NcoI at the 5′ end and StuI at the 3′ end and ligated into the pHBT vector with HA, Flag, or GFP sequences at the 3′ end to generate pHBT-NUT-Flag/HA/GFP. The pHBT-35S::NUT^{K714E}-HA vector was generated by site-directed mutagenesis using pHBT-35S::NUT-HA as the template.

To construct pSCREW::GUS vectors, 1,879-bp and 1,927-bp sequences upstream of the *SCREW1* or *SCREW2* start codon were amplified from genomic DNAs using the primer pair containing HindIII or BglII and ligated into the pGFPGUSplus vector[23]. *SCREW1* or *SCREW2* were PCR-amplified using gene-specific primers containing KpnI or SalI, followed by KpnI and SalI digestion and ligation into the pCAMBIA1300 vector to generate pCAMBIA1300-35S::SCREW1, 2. *SCREW1* was amplified using gene-specific primers containing XhoI or StuI and inserted into pTA7002 with an HA-tag at the 3′ end to generate pTA7002-Dex::SCREW1-HA. SCREW1-HA-NOS was then shuttled to the pTK103 vector by XhoI and SpeI digestion to create pTK103-Est::SCREW1-HA. Coding sequences of *SCREW1*, *SCREW2*, *NUT*, and *ABI2* were PCR-amplified from *Arabidopsis* cDNA using gene-specific primers with overlapping sequences from the pMDC32-GFP or pMDC32-HA vector and then were recombined into the BamHI- and StuI-digested pMDC32-35S::GFP or pMDC32-35S::HA using the ClonExpress II One Step Cloning Kit (Vazyme) to generate pMDC32-35S::SCREW1/2, NUT-GFP, and pMDC32-35S::ABI2. *ABI1* and *OST1* were PCR-amplified from Col-0 cDNA using gene-specific primers with BamHI at the 5′ end and StuI at the 3′ end, followed by digestion with BamHI and StuI and ligation into the pMDC32 vector with the HA or Flag sequence at the 3′ end to generate pMDC32-35S::ABI1-HA and pMDC32-OST1-Flag.

To create the *E. coli* recombinant protein constructs, the coding sequences of SCREWs without the N-terminal signal peptide were PCR-amplified from *Arabidopsis* cDNA using gene-specific primers with BamHI or XhoI and inserted into pGEX-4T-1 to generate pGST-SCREW1, 2, 3. The *SCREW1* coding sequence lacking the N-terminal signal peptide was PCR-amplified from cDNAs using gene-specific primers containing BamHI or StuI and inserted into pET28a-His-SUMO-BIK1 to create pET28a-His-SUMO-SCREW1. ABI1-HA was PCR-amplified from pMDC32-35S::ABI1-HA using gene-specific primers containing BamHI or StuI and inserted into pET28a-His-SUMO-BIK1 to create pET28a-His-SUMO-ABI1-HA. The cytosolic domain of NUT (NUT_{CD}) was PCR-amplified from *Arabidopsis* cDNA using gene-specific primers with BamHI or XhoI and inserted into pGEX-4T-1 to create pGST-NUT_{CD}. pGST-NUT_{CD}(K714E) was generated by site-directed mutagenesis using pGST-NUT_{CD} as a template. To build the construct used for recombinant NUT_{ECD} expression in insect cells, the nucleotide sequence encoding NUT_{ECD} (aa residues 23–626) was biosynthesized and cloned into the pFastBac-1 vector with a signal peptide (MKLCILLAVVAFVGLSLG) at the N terminus and a 6×His tag at the C terminus (Gene Universal).

To construct pHEE401E-gSCREW1-gSCREW2 for the CRISPR–Cas9-mediated gene editing, two guide RNAs (gRNAs) were designed using CHOPCHOP (http://chopchop.cbu.uib.no/). gRNA1 targeting *SCREW1* and gRNA2 targeting *SCREW2* were incorporated into a gRNA expression cassette through PCR amplification with primers carrying gRNA1, gRNA2, and pCBC-DT1T2 as a template. The PCR fragments were further amplified using primers containing BsaI and inserted into pHEE401E[55].

All primers are listed in Supplementary Table 1, and PCR-amplified DNA fragments were confirmed using Sanger sequencing.

Protoplast isolation and transient expression assays were described previously[56]. *Agrobacterium tumefaciens* strain GV3101 carrying binary vectors was used for *Arabidopsis* transformation by floral dipping. Transformants were selected with 25 μg ml^{-1} hygromycin, 50 μg ml^{-1} kanamycin or 10 μg ml^{-1} Basta. Multiple transgenic lines were analysed by immunoblotting for protein expression. Two lines with the 3:1 segregation ratio for antibiotic resistance in the T_3 generation were selected to obtain homozygous seeds for further studies.

Peptide synthesis

Peptide sequences were listed in Supplementary Table 2. Flg22 and Pep1 were synthesized from BIOMATIK (Delaware), and SCREWs and SCREW derivatives from ChinaPeptides. For the synthesis of N-terminally biotinylated SCREW1 (biotin–SCREW1), a lysine residue was added to the N terminus of the SCREW1 peptide, and biotin was bound to the lysine side chain through an amide bond. For the synthesis of SCREW2(CC), SCREW2 peptide was oxidized with the addition of 10% DMSO (v/v) to facilitate the formation of a disulfide bond at pH 8.0 adjusted by meglumine.

Identification of *screw1/2* mutants

Genomic DNAs were extracted from wild-type plants and T_1 generation pHEE401E-gSCREW1-gSCREW2 transformants. Fragments of 672 bp for *SCREW1* and 679 bp for *SCREW2* spanning the targeted loci of the gRNAs were amplified and subjected to BslI digestion. Gene editing in the fragments was confirmed by Sanger sequencing. Transgenic plants containing mutations in both *SCREW1* and *SCREW2* were used for further analyses. T_2 and T_3 plants were further confirmed by BslI digestion and Sanger sequencing.

RNA isolation, reverse transcription and RT–qPCR analysis

Total RNAs were extracted from *Arabidopsis* seedlings or rosette leaves using TRIzol reagent (Invitrogen) and quantified with a spectrophotometer (NanoDrop2000, Thermo Fisher Scientific). One microgram of total RNAs were reverse-transcribed to synthesize the first-strand cDNA with M-MuLV Reverse Transcriptase and oligo(dT) primers after treatment with RNase-free DNase I (New England Biolabs). RT–qPCR analyses were performed in the CFX384 Touch Real-Time PCR Detection

System (Bio-Rad) with gene-specific primers (Supplementary Table 1) and iTaq SYBR green Supermix (Bio-Rad) following a manufactural protocol. The expression of each gene was normalized to the expression of *UBQ10* or *ACTIN2*.

MAPK activation assay

Ten-day-old seedlings grown on ½MS plates were transferred into ddH_2O, kept overnight, and then treated with flg22, Pep1 or SCREWs with the indicated concentrations for the indicated time. Each sample containing three seedlings was grounded in 40 µl extraction buffer (150 mM NaCl, 50 mM Tris-HCl, pH 7.5, 5 mM EDTA, 1% [v/v] Triton X-100, 1 mM Na_3VO_4, 1 mM NaF, 1 mM DTT and 1:200 complete protease inhibitor cocktail from Sigma). The supernatant was collected after 13,000*g* centrifugation for 5 min at 4 °C, and protein samples with 1× SDS buffer were loaded on 10% (v/v) SDS–PAGE gel to detect phosphorylated MPK3 and MPK6 by immunoblotting with anti-pERK1/2 antibodies (1:2,000; Cell Signaling) followed by anti-rabbit (1:10,000; Cell Signaling).

Analysis of ROS production

The third or fourth pair of true leaves from four- to five-week-old soil-grown *Arabidopsis* plants were excised into leaf discs (5 mm diameter). Leaf discs were incubated in 100 µl ddH_2O in a 96-well plate with gentle shaking overnight to eliminate the wounding effect. Water was replaced by 100 µl of a reaction solution containing 50 µM luminol, and 10 µg ml^{-1} horseradish peroxidase (HRP, Sigma-Aldrich) supplemented with or without 100 nM flg22, 100 nM or 1 µM SCREW1. Luminescence was measured with a luminometer (Glomax Multi-Detection System, Promega) for 40 min. ROS production was indicated as means of relative light units (RLU).

Quantitative Ca^{2+} measurements

Protoplasts were transfected with p35S::mCherry-AEQ[57] and incubated in WI solution (0.5 M mannitol, 20 mM KCl and 4 mM MES pH 5.7) supplemented with 2 mM $CaCl_2$ at 23 °C for 7 h, followed by a 2-h treatment with 10 µM coelenterazine-h (Thermo Fisher Scientific). Approximately 2×10^4 protoplasts (100 µl with a density of 2×10^5 cells per ml) were loaded into individual wells of a black 96-well microplate and incubated for 30 min in the dark followed by treatment with flg22 or SCREW1 and Ca^{2+} measurements. Luminescence was measured with a luminometer (Glomax Multi-Detection System, Promega) with a 1-s interval for 15 min. The values for cytosolic Ca^{2+} concentration were indicated as means of RLU.

Seedling growth inhibition assay

Three-day-old seedlings grown on vertical ½MS plates were transferred into a 24-well plate containing 500 µl liquid ½MS medium supplemented with or without 1 µM SCREWs. Two seedlings were placed in a single well, and a total of at least six seedlings was used for each treatment. Seedlings were photographed seven days after treatments, and the fresh weight of each seedling was measured.

Trypan blue staining

Trypan blue staining was performed as previously described with modifications[48]. In brief, detached leaves were immersed in the trypan blue staining solution (2.5 mg ml^{-1} trypan blue in lactophenol (lactic acid:glycerol:liquid phenol:H_2O = 1:1:1:1]) under vacuum infiltration for 5 min, followed by incubation at 23 °C for 8 h with shaking at 70 r.p.m. on a rocker. Leaves were destained in a solution (ethanol: lactophenol = 2:1) at 65 °C for 30 min and then incubated in fresh distaining solution 23 °C until completely destained.

Toluidine blue staining

Toluidine blue staining was performed as previously described[34]. Shoots of three-week-old plants grown in soil were submerged in 0.05% toluidine blue solution at room temperature for 15 min. Abaxial surfaces of plant leaves from four-week-old plants were dipped with 5 µl of 0.05% toluidine blue solution and incubated for 5–60 min at room temperature. The samples were rinsed with water before being photographed.

Histochemical detection of GUS activity

Two-week-old *Arabidopsis* seedlings or rosette leaves of four-week-old plants were immersed and vacuumed in the GUS staining solution (10 mM EDTA, 0.01% Silwet L-77, 2 mM $K_3Fe(CN)_6$, 2 mM $K_4Fe(CN)_6$ and 2 mM X-Gluc in 50 mM PBS, pH 7.0) for 5 min, followed by incubation at 37 °C for 12–24 h. Samples were cleared in 75% ethanol for 6 h, followed by photographing using the Olympus SZX10 stereomicroscope.

FRK1 reporter assay

For detection of flg22- or SCREW-induced *FRK1* promoter activity, protoplasts (100 µl at the concentration of 10^5 cells per ml) of wild-type Col-0 were co-transfected with 8 µg of pFRK1::LUC and 2 µg of pUBQ10::GUS, aliquoted into individual wells to incubate for 4 h at 23 °C followed by treatment with 100 nM flg22, 1 µM GST or 1 µM GST–SCREW for another 4 h. For *NUT* complementation assays, protoplasts of wild-type Col-0 and *nut* mutants were co-transfected with pFRK1::LUC, pUBQ10::GUS, and an empty vector or p35S::NUT-HA as described above. Protoplasts were collected and lysed with 30 µl cell lysis buffer (25 mM Tris-HCl, pH 7.5, 2 mM EDTA, 10% (v/v) glycerol, 1% (v/v) Triton X-100 and 2 mM DTT). Cell lysates (20 µl) were used for the detection of luciferase activity with the Glomax Multi-Detection System (Promega) and the luciferase assay substrate (Promega). For GUS activities, 4-MUG (4-methylumbelliferyl-β-D-glucuronide) was mixed with 10 µl cell lysates, and fluorescence signals were analysed with a Multilabel Plate Reader (Victor X3, PerkinElmer). The relative luciferase activity was indicated by the ratio of the activity of luciferase to GUS.

Laser confocal microscopy

For protoplast transient expression assay, protoplasts were transfected with pHBT-35S::GFP, pHBT-35S::NUT-GFP or pHBT-35S::FLS2-GFP and incubated for 12 h. For *N. benthamiana* transient expression assays, *A. tumefaciens* strain GV3101 containing pMDC32-35S::GFP, pMDC32-35S::SCREW2-GFP, or pMDC32-35S::NUT-GFP was cultured overnight in LB medium (10 g l^{-1} tryptone, 5 g l^{-1} yeast extract, 5 g l^{-1} NaCl) at 28 °C. The bacterial suspension containing 10 mM MES, pH 5.7, 10 mM $MgCl_2$ and 200 µM acetosyringone at an optical density at 600 nm ($OD_{600\,nm}$) of 1.0 was infiltrated into leaves of four-week-old soil-grown *N. benthamiana* using a needleless syringe and incubated for 72 h. To detect SCREW1-induced NUT endocytosis, true leaves of seven-day-old *Arabidopsis* transgenic seedlings carrying pMDC32-35S::NUT-GFP were treated with water or 100 nM SCREW1 for 5 and 45 min and imaged using the Leica SP8 confocal laser microscope. The cotyledons of ten-day-old transgenic seedlings carrying p35S::GFP or p35S::NUT-GFP grown on $^1/_2$MS plates were used to observe GFP and NUT–GFP subcellular localization. Fluorescence images were taken with the Leica SP8 confocal laser microscope. The excitation laser of 488 nm and 561 nm was used for imaging GFP and chloroplast fluorescence, respectively.

Transmission electron microscopy

Leaves of four-week-old plants were fixed in 3.7% formaldehyde and 1% glutaraldehyde in PBS buffer. After primary fixation, samples were rinsed and postfixed in buffered 1% osmium tetroxide. Samples were then dehydrated in an acetone series and embedded in Quetol-ERL 421 resin. The sectioned samples were imaged on a JEOL1200Ex electron microscope.

In vivo co-immunoprecipitation assays

For co-IP in protoplasts, protoplasts were co-transfected with the indicated vectors and incubated for 12 h. After treatment with 1 µM SCREWs or flg22 for 15 min, protoplasts were collected by centrifugation at 100*g* for 2 min and lysed in 300 µl of IP buffer (20 mM Tris-HCl, pH7.5,

100 mM NaCl, 1 mM EDTA, 10% (v/v) glycerol, 0.5% (v/v) Triton X-100 and protease inhibitor cocktail from Sigma) by vortexing. After centrifugation at 10,000*g* for 10 min at 4 °C, 30 µl of supernatant was collected as input control. The remaining supernatant was pre-incubated with protein G–agarose beads at 4 °C for 1 h with gentle shaking at 70 r.p.m. on a rocker. Immunoprecipitation was performed with anti-Flag agarose (Sigma-Aldrich) for 3 h at 4 °C. Beads were collected by centrifugation at 500*g* for 2 min and washed three times with washing buffer (20 mM Tris-HCl, pH 7.5, 100 mM NaCl, 1 mM EDTA, 0.1% (v/v) Triton X-100) and once with 50 mM Tris-HCl, pH 7.5. Immunoprecipitated proteins and input proteins were analysed by immunoblotting with anti-HA (1:2,000; Roche) or anti-Flag antibodies (1:2,000; Sigma-Aldrich).

For biotin-labelled SCREW1 (biotin–SCREW1) immunoprecipitation with NUT–Flag, protoplasts were transfected with p35S:: NUT-Flag, p35S::FLS2-Flag or an empty vector (control) and incubated for 12 h. Samples were lysed with lysis buffer as indicated above and incubated with 100 nM biotin–SCREW1 at 4 °C with shaking at 70 r.p.m. on a rocker for 3 h. Ten micromoles of non-labelled SCREW1 or flg22 was added together with biotin–SCREW1 as competitors. Five microlitres of anti-Flag agarose beads was added into the samples and they were incubated for another 1 h at 4 °C. Agarose beads were collected by centrifugation at 500*g* for 2 min and washed three times with the aforementioned washing buffer and one time with 50 mM Tris-HCl, pH 7.5. Immunoprecipitated proteins and input proteins were analysed by immunoblotting with anti-Flag antibodies (1:2,000; Sigma-Aldrich) for NUT–Flag and FLS2–Flag and HRP-labelled streptavidin (1:5,000; Thermo Fisher Scientific) for biotin–SCREW1.

For co-immunoprecipitation in plants, ten-day-old transgenic seedlings carrying p35S::GFP or p35S::NUT-GFP grown on the liquid $^1/_2$MS were treated with or without SCREW1 or SCREW2 for 15 min. Seedlings of 500 mg were ground into powders with liquid nitrogen and lysed in 2 ml IP buffer by vortexing. After centrifugation at 10,000*g* for 10 min at 4 °C, the supernatant was collected for incubation with GFP-trap beads (Chromotek, Germany) at 4 °C for 3 h with gentle shaking at 70 r.p.m. on a rocker. Beads were collected by centrifugation at 500*g* for 2 min and washed three times with washing buffer (20 mM Tris-HCl, pH 7.5, 100 mM NaCl, 1 mM EDTA, 0.1% (v/v) Triton X-100) and once with 50 mM Tris-HCl, pH 7.5. Immunoprecipitated proteins and input proteins were analysed by immunoblotting with anti-GFP (1:2,000, Roche) followed by anti-mouse (1:10,000, Cell Signaling) or anti-BAK1 antibodies (1:2,000)[58] followed by anti-rabbit (1:10,000, Cell Signaling).

Disease assays

For bacteria disease assays, *Pst* DC3000, *Pst* DC3000 *hrcC*$^-$, *Pst* DC3000 *avrRpm1* and *Pst* DC3000 *avrRpt2* were cultured in King's B (KB) liquid medium (Bacto proteose peptone 20 g l^{-1}, K_2HPO_4 1.5 g l^{-1}, $MgSO_4{\cdot}7H_2O$ 1.5 g l^{-1}, glycerol 20 ml l^{-1} and agar 15 g l^{-1}, pH 7.2) containing 50 µg ml^{-1} rifampicin at 28 °C for 12 h. The bacteria were collected by centrifugation at 2,000*g* for 2 min at 23 °C and diluted into the indicated titres with 10 mM $MgCl_2$. Fully expanded leaves of four-week-old plants were spray inoculated or infiltrated with the bacterial suspension using a 1-ml needleless syringe. For flg22 or SCREW1-mediated protection assays, leaves were infiltrated with 500 nM flg22 or SCREW1 24 or 36 h before inoculation with *Pst* DC3000. Leaf disks were collected for the bacterial counting at 0 or 3 days post-inoculation (dpi). Bacteria in two leaf disks as one sample were released into 200 µl H_2O by grinding, diluted into gradient titres and spread on tryptone soya agar (TSA) plates (1% (w/v) Bacto tryptone, 1% (w/v) sucrose, 0.1% (w/v) glutamic acid and 1.5% (w/v) agar) containing 25 µg ml^{-1} rifampicin. Bacterial colonies were counted to determine colony-forming units (cfu) after incubation at 28 °C for two days.

For *Botrytis cinerea* disease assays, the *B. cinerea* strain BO5-10 was inoculated on potato dextrose agar and cultivated at 23 °C for two days. Conidia were collected and diluted to 10^7 spores per ml with potato dextrose broth. Leaves detached from four-week-old plants were dropped with 5 µl spore suspension and kept in 98% humidity. Diameters of disease spots were measured at 2 dpi.

Aphid bioassays

Aphid no-choice tests were performed as described previously[59]. Green peach aphids (*Myzus persicae*) used in this study are a tobacco (*Nicotiana tabacum*)-adapted red lineage that were maintained on cabbage (*Brassica oleracea*). Both adults and nymphs used in our experiments were female. Six age-synchronized second-instar nymphs (within 24 h) were placed on four-week-old plants. The total number of neonates on each plant was counted 10 days after infestation. Each genotype had at least 10 replicates.

Measurement of stomatal aperture

Stomatal apertures were measured on epidermal peels excised from the abaxial side of leaves of three- to four-week-old plants as described previously[60,61]. For detection of flg22, ABA or SCREW1 induction of stomatal closure, two epidermal peels from two independent plants were incubated for 30 min in the dark in a bathing solution containing 30 mM KCl and 10 mM MES/Tris, pH 6.0. Epidermal peels were first maintained under darkness to keep them closed or exposed to white light in a growth chamber (120 µE m^{-2} s^{-1}) for 3 h to induce maximal stomatal opening. Then, flg22 (1 µM), ABA (10 µM), SCREW1 (1 µM) or a combination of SCREW1 and flg22 or ABA was added to the bathing solution, and stomatal apertures were monitored for the indicated time in over 60 stomata for each independent repetition. The width and the length of the stomatal aperture were measured using ImageJ, and the stomatal aperture index was calculated by division of the aperture width through the length as described[62].

Measurement of stomatal conductance

Stomatal conductance in leaves of six-week-old *Arabidopsis* plants was measured using a portable photosynthesis system (CIRAS-3, PP Systems). For detection of stomatal conductance under pathogen infections, the sixth or seventh pairs of true leaves were hand-inoculated with *Pst* DC3000 ($OD_{600\,nm}$ = 0.01) after exposure under light (120 µE m^{-2} s^{-1}) for 2 h in the growth chamber, and stomatal conductance was measured at the indicated time point. Measurement parameters were CO_2 400 µmol mol^{-1} and photosynthetic photon flux density of 200 µmol m^{-2} s^{-1}.

Measurement of water potential

Measurement of water potential was achieved with the water-responding pProU::GFP reporter described previously with modifications[33]. The plasmid carrying pProU::GFP or pNptII::GFP was transformed into *Pst* DC3000. To measure the water potential, leaves from four-week-old soil-grown *Arabidopsis* plants were hand-inoculated with *Pst* DC3000 pProU::GFP or *Pst* DC3000 pNptII::GFP ($OD_{600\,nm}$ = 0.1), respectively. Two leaf discs were then collected at 0, 3, 6, and 9 h post-inoculation, and proteins were extracted with 1× SDS loading buffer. The expression of GFP in leaf discs was detected by immunoblotting with anti-GFP antibody (1:2,000; Roche) followed by anti-mouse (1:10,000; Cell Signaling) and quantified by ImageJ. Quantification data are shown as the ratio of signal intensities of pProU::GFP to pNptII::GFP.

Patch-clamp experiments

S-type anion channel recordings were performed as previously described[63,64]. *Arabidopsis* guard cell protoplasts were isolated from the epidermis of rosette leaves by a 12-h incubation at 21 °C with shaking in an enzyme solution containing 1.0% (w/v) Cellulase R10 (Yakult Pharmaceutical Industry), 0.5% (w/v) Macerozyme R10 (Yakult Pharmaceutical Industry), 0.5% (w/v) bovine serum albumin, 0.1% (w/v) kanamycin, 0.1 mM KCl, 0.1 mM $CaCl_2$, 10 mM ascorbic acid and 500 mM D-mannitol (pH 5.6 with KOH). Isolated guard cell protoplasts were collected through a nylon mesh with 10 µm size openings and then

washed twice by centrifugation at 200*g* for 5 min with wash solution containing 0.1 mM KCl, 0.1 mM $CaCl_2$ and 500 mM D-sorbitol (pH 5.6 with KOH). Guard cell protoplasts were treated with or without 5 μM SCREW1 for 1 h, followed by treatment with or without 10 μM ABA for 0.5 h. The patch-clamp pipette solution was composed of 150 mM $CsCl_2$, 2 mM $MgCl_2$, 6.7 mM EGTA, 5.58 mM $CaCl_2$, 5 mM Mg-ATP and 10 mM HEPES-Tris (pH 7.1). The patch-clamp bath solution was composed of 30 mM $CsCl_2$, 2 mM $MgCl_2$, 1 mM $CaCl_2$ and 10 mM MES-Tris (pH 5.6). Osmolarities of the pipette and bath solutions were adjusted with D-sorbitol to 500 mosmol kg^{-1} and 485 mosmol kg^{-1}, respectively. Whole-cell S-type anion current recordings were performed using a CEZ-2200 patch-clamp amplifier (Nihon Kohden) and pCLAMP 8.1 software (Molecular Devices).

ABA and mannitol treatment and measurement of water loss

For measurement of water loss, rosette leaves were detached from four-week-old plants and laid on dry filter paper under the light with the abaxial side of the leaves facing up. The weights of leaves were measured every hour over a period of six hours. The water-loss rate was presented as the leaf weight ratio at each time point relative to the initial weight. For analyses of the effects of ABA treatment on cotyledon greening rate, seeds after stratification at 4 °C for two days were germinated on ½MS plates with or without 1 μM ABA for seven days; this was followed by photographing, and the percentages of seedlings with radical and expanded green cotyledons were calculated. Approximately 80 seeds were counted for each genotype in each biologically independent repeat. For analyses of mannitol-treated phenotypes, seeds were germinated on ½MS plates containing 3 μM β-oestradiol supplemented with or without 100 or 200 mM mannitol after surface sterilization and stratification. Seedlings were photographed after 15 days of growth.

Purification of recombinant proteins, GST pull-down and in vitro kinase and phosphatase assays

Recombinant proteins were expressed in *E. coli* BL21 strain with an isopropyl β-D-1-thiogalactopyranoside (IPTG)-inducible system. GST and GST-tagged proteins were purified with Pierce glutathione agaroses (Thermo Fisher Scientific), and His-tagged proteins were purified with Ni Sepharose beads (Qiagen) according to manufacturer's protocol. For the GST pull-down assay, 10 mg of His–ABI1–HA proteins were incubated with prewashed GST or GST–NUT_{CD} glutathione beads in 0.5 ml pull-down buffer (10 mM HEPES (pH 7.5), 100 mM NaCl, 1 mM EDTA, 10% glycerol and 1% Triton X-100) for 2 h at 4 °C with gentle shaking. The pulled-down proteins were analysed by immunoblotting with anti-HA (1:2,000) antibodies. For in vitro kinase assays, GST, GST–NUT_{CD} or GST–NUT_{CD}(K714E) were incubated in a kinase reaction buffer (20 mM Tris-HCl, pH 7.5, 20 mM $MgCl_2$, 5 mM EDTA, 1 mM DTT and 100 mM ATP) containing 5 μCi [γ-^{32}P]ATP for 2 h at 23 °C with gentle shaking. The reaction was stopped by adding 4× SDS loading buffer (250 mM Tris-HCl, pH 6.8, 40% (v/v) glycerol, 4% (w/v) SDS, 0.1% (w/v) bromophenol and 4% (v/v) β-mercaptoethanol). Protein phosphorylation was visualized by autoradiography after running with SDS–PAGE. For in vitro phosphatase assay, protoplasts were transfected with pMDC32-35S::ABI1-HA and incubated for 12 h. After treatment with 1 μM SCREW1 for 5 min, protoplasts were collected by centrifugation at 100*g* for 2 min and lysed in 300 μl of IP buffer by vortexing. ABI1–HA was immunoprecipitated from the supernatant with anti-HA magnetic beads (Thermo Fisher Scientific) and resuspended in IP buffer. ABI1–HA and MBP–OST1 were incubated in a kinase reaction buffer containing 5 μCi [γ-^{32}P]ATP for 2 h at 23 °C with gentle shaking. The reaction was stopped by adding 4× SDS loading buffer. MBP–OST1 phosphorylation was visualized by autoradiography after 10% SDS–PAGE. Band intensities of phosphorylated MBP–OST1 (pOST1) normalized to input MBP–OST1 were quantified by ImageJ, and averages of three independent repeats were labelled below the gel ($n = 3$, biologically independent repeats).

Phos-tag immunoblotting

For detecting the phosphorylation of ABI1, ABI2 or OST1 with Phos-tag gel, protoplasts were transfected with pMDC32-35S::ABI1/2-HA or pMDC32-35S::OST1-Flag and incubated for 12 h. After treatment with SCREW or ABA, protoplasts were collected by centrifugation at 100*g* for 2 min and then lysed with 1× SDS loading buffer. The total proteins were separated in the 8% SDS–PAGE containing 25 μM Phos-tag (Fujifilm Wako Chemicals) and 100 mM $MnCl_2$, and immunoblotted with anti-HA (1:2,000) or anti-Flag antibodies (1:2,000, Sigma-Aldrich). For certain Phos-tag SDS–PAGE, molecular weight cannot be exactly indicated. For relative pABI1, band intensities of phosphorylated ABI1 (pABI1) normalized to input ABI1 in regular immunoblotting were quantified. For relative pOST1, band intensities of phosphorylated OST1 (pOST1) and unphosphorylated OST1 were quantified by ImageJ and the relative pOST1 represents the ratio of phosphorylated to unphosphorylated OST1.

NUT_{ECD} expression in insect cells and SPR analyses

NUT_{ECD} fused with a signal peptide (MKLCILLAVVAFVGLSLG) at the N terminus and a 6× His at the C terminus was expressed using the Bac-to-Bac baculovirus expression system (Invitrogen) in SF9 cells (Thermo Fisher Scientific, cat. no. 11496015) at 27 °C. No additional authentication or mycoplasma contamination testing was done by authors in this study. Five hundred millilitres of SF9 cells (2×10^6 per ml) cultured in the Sf-900 II SFM medium (Invitrogen) were infected with 25 ml recombinant baculovirus and were cultured for another four days with gentle shaking at 27 °C. Secreted NUT_{ECD} in the supernatant was purified with Ni-NTA beads (Novagan) and then was dialysed into 10 mM PBS solution (2 mM KH_2PO_4, 8 mM Na_2HPO_4, 136 mM NaCl, 2.6 mM KCl, pH 7.4). Expression and purification of $BAK1_{ECD}$ protein (residues 1–220) were described previously[65].

The binding kinetics and affinities of NUT_{ECD} with SCREW or SCREW derivative peptides were performed on a Biacore T200 instrument (GE Healthcare) with CM5 chips (GE Healthcare) at 25 °C. NUT_{ECD} proteins were exchanged to 10 mM NaAc (pH 5.0) and the peptides were dissolved in HBS-EP+ (10 mM HEPES, 150 mM NaCl, 3 mM EDTA and 0.05% (v/v) Surfactant P20, pH 7.5 or pH 5.7) (GE Healthcare). About 4,700 response units of NUT_{ECD} proteins were immobilized on the CM5 chip, and a blank channel was used as a negative control. The peptides were diluted into indicated concentrations and injected at a flow rate of 30 μl min^{-1} in the absence or presence of 0.1 μM $BAK1_{ECD}$ for 120 s, followed by dissociation for 5 min. After dissociation, 5 mM NaOH was injected for 30 s to remove any non-covalently bound proteins from the chip surface. The binding kinetics were analysed with the software Biaevaluation v.4.1 using the 1:1 Langmuir binding mode.

Multiple sequence alignment and phylogenetic tree analysis

Protein sequences were accessed from the NCBI database. Amino acid sequences were aligned using ClustalW and visualized in ESPript3 (https://espript.ibcp.fr/ESPript/ESPript/). WebLogo was conducted with WebLogo 3 (http://weblogo.threeplusone.com/). Phylogenetic trees were constructed using MEGAX with the neighbour-joining method. The trees in Extended Data Figs. 1b, c, 5b, 5c were visualized in an interactive tree of life (iTOL, https://itol.embl.de/).

Quantification and statistical analysis

No statistical methods were used to predetermine sample size. Blinding and randomization were not used. Data for quantification analyses are presented as mean ± s.e.m. or standard deviation (s.d.), or as box plots with the interquartile range as the upper and lower confines, minima and maxima as whiskers, and the median as a solid line. Statistical analyses were performed by two-sided Student's *t*-test, or one-way or two-way ANOVA followed by Tukey's or Dunnett's test. The number of biologically independent replicates is indicated in graphs or figure legends. Exact *P* values are provided in the graphs and Supplementary Table 3.

Reporting summary

Further information on research design is available in the Nature Research Reporting Summary linked to this paper.

Data availability

The data supporting the findings of this study are available within the paper and its Supplementary Information files (uncropped blots and gel images, primers, peptides, and exact *P* values). The sequences of proteins were obtained from TAIR (https://www.arabidopsis.org/), UniProt (https://www.uniprot.org/), NCBI (https://www.ncbi.nlm.nih.gov/) and Phytozome (https://phytozome-next.jgi.doe.gov/). The protein structures were obtained from AlphaFold Protein Structure Database (https://alphafold.ebi.ac.uk/). Sequence data from this article can be found in the *Arabidopsis* Genome Initiative or GenBank–EMBL databases under the following accession numbers: *SCREW1* (AT1G06135), *SCREW2* (AT2G31345), *SCREW3* (AT1G06137), *SCREW4* (AT2G31335), *NUT* (AT5G25930), *WRKY30* (AT5G24110), *WRKY33* (AT2G38470), *WRKY53* (AT4G23810), *PR1* (AT2G14610), *FRK1* (AT2G19190), *MPK3* (AT3G45640), *MPK4* (AT4G01370), *MPK6* (AT2G43790), *UBQ10* (AT4G05320), *ACTIN2* (AT3G18780), *BAK1* (AT4G33430), *SERK1* (AT1G71830), *SERK2* (AT1G34210), *SERK4* (AT2G13790), *FLS2* (AT5G46330), *BIK1* (AT2G39660), *MIK2* (AT4G08850), *MIK2L* (AT1G35710), *RLK7* (AT1G09970), *IKU2* (AT3G19700), *HAE* (AT4G28490), *HSL2* (AT5G65710), *LET1* (AT2G23200), *LET2* (AT5G38990), *NILR1* (AT1G74360), *MIN7* (AT3G43300), *ABI1* (AT4G26080), *ABI2* (AT5G57050) and *OST1* (AT4G33950).

49. Meng, X. et al. Ligand-induced receptor-like kinase complex regulates floral organ abscission in *Arabidopsis*. *Cell Rep.* **14**, 1330–1338 (2016).
50. Li, B. et al. Phosphorylation of trihelix transcriptional repressor ASR3 by MAP KINASE4 negatively regulates *Arabidopsis* immunity. *Plant Cell* **27**, 839–856 (2015).
51. de Oliveira, M. V. V. et al. Specific control of Arabidopsis BAK1/SERK4-regulated cell death by protein glycosylation. *Nat. Plants* **2**, 15218 (2016).
52. Li, L. et al. TMK4 receptor kinase negatively modulates ABA signaling by phosphorylating ABI2 and enhancing its activity. *J. Integr. Plant Biol.* **63**, 1161–1178 (2021).
53. Wu, Y. et al. Genome-wide expression pattern analyses of the *Arabidopsis* leucine-rich repeat receptor-Like kinases. *Mol. Plant* **9**, 289–300 (2016).
54. Li, F. et al. Modulation of RNA polymerase II phosphorylation downstream of pathogen perception orchestrates plant immunity. *Cell Host Microbe* **16**, 748–758 (2014).
55. Yu, X. et al. The receptor kinases BAK1/SERK4 regulate Ca^{2+} channel-mediated cellular homeostasis for cell death containment. *Curr. Biol.* **29**, 3778–3790 (2019).
56. He, P., Shan, L. & Sheen, J. in *Plant–Pathogen Interactions* (ed. Ronald, P. C.) 1–9 (Humana Press, 2007).
57. Maintz, J. et al. Comparative analysis of MAMP-induced calcium influx in *Arabidopsis* seedlings and protoplasts. *Plant Cell Physiol.* **55**, 1813–1825 (2014).
58. Zhou, J. et al. Proteolytic processing of SERK3/BAK1 regulates plant immunity, development, and cell death. *Plant Physiol.* **180**, 543–558 (2019).
59. Lei, J. et al. BOTRYTIS-INDUCED KINASE1 modulates *Arabidopsis* resistance to green peach aphids via PHYTOALEXIN DEFICIENT4. *Plant Physiol.* **165**, 1657–1670 (2014).
60. Rodrigues, O. et al. Aquaporins facilitate hydrogen peroxide entry into guard cells to mediate ABA- and pathogen-triggered stomatal closure. *Proc. Natl Acad. Sci. USA* **114**, 9200–9205 (2017).
61. Babilonia, K. et al. A nonproteinaceous *Fusarium* cell wall extract triggers receptor-like protein-dependent immune responses in *Arabidopsis* and cotton. *New Phytol.* **230**, 275–289 (2021).
62. Eisele, J. F., Fassler, F., Burgel, P. F. & Chaban, C. A rapid and simple method for microscopy-based stomata analyses. *PLoS One* **11**, e0164576 (2016).
63. Brandt, B. et al. Calcium specificity signaling mechanisms in abscisic acid signal transduction in Arabidopsis guard cells. *eLife* **4**, e03599 (2015).
64. Munemasa, S. et al. Ethylene inhibits methyl jasmonate-induced stomatal closure by modulating guard cell slow-type anion channel activity via the OPEN STOMATA 1/SnRK2.6 kinase-independent pathway in *Arabidopsis*. *Plant Cell Physiol.* **60**, 2263–2271 (2019).
65. Sun, Y. et al. Structural basis for flg22-induced activation of the Arabidopsis FLS2–BAK1 immune complex. *Science* **342**, 624–628 (2013).

Acknowledgements We thank the *Arabidopsis* Biological Resource Center (ABRC) and the Nottingham *Arabidopsis* Stock Centre (NASC) for providing the *Arabidopsis* T-DNA insertion lines; G. A Beattie for sharing water potential reporters, bacterial strains and assay protocols; R. Panstruga for the p35S::mCherry-AEQ construct; F. Yu for providing *abi1-2/abi2-2* mutants; J. Chai and Z. Han for providing $BAK1_{ECD}$ proteins; and J. Li for providing pNUT::GUS seeds. We also thank J. Schroeder and P.-K. Hsu for help with the stomatal conductance experiment and for critical reading of the manuscript, and members of the laboratories of L.S. and P.H. for discussions and comments on the experiments. The work was supported by the National Science Foundation (NSF) (IOS-1951094) and the National Institutes of Health (NIH) (R01GM092893) to P.H.; the NIH (R35GM144275), the NSF (IOS-2049642) and the Robert A. Welch Foundation (A-2122) to L.S.; the National Natural Science Foundation of China (NSFC) (31500971), the Youth Innovation Technology Project of Higher School in Shandong Province (2020KJF013) and the Natural Science Foundation of Shandong Province (ZR2020MC022) to S.H.; the Science and Technology Development Program of Shandong Province (2012GSF11712) to H.W.; and the Natural Science Foundation of Shandong Province (ZR201807100168) to W.Z.

Author contributions S.H., Z.L., L.S. and P.H. conceived the project, designed experiments and analysed data. Z.L. and S.H. performed most of the experiments. O.R. performed stomatal movement assays. P.W. constructed the *Pst* DC3000 reporter strains and contributed to water potential assays. D.L. contributed to observations of the subcellular localization of SCREW and NUT, and to the GUS staining assays. S.M. performed the patch-clamp experiment. J. Lei in the laboratory of K.Z.-S. performed aphid bioassays. K.N. in the laboratory of S.Y.H. contributed to *min7* disease assays. X.W. in the laboratory of W.Z. built p35S::SCREW1/2 transgenic lines. J. Liu contributed to the NUT or FLS2 and SERK interaction assays. F.A.O.-M. contributed to SCREW and NUT binding and endocytosis assays. C.Y. contributed to genotyping and *Arabidopsis* transformation. S.Y.H., K.Z.-S., W.Z. and H.W. analysed data and provided critical feedback; L.S., P.H., S.H. and Z.L. wrote the manuscript with input from all authors.

Competing interests The authors declare no competing interests.

Additional information
Supplementary information The online version contains supplementary material available at https://doi.org/10.1038/s41586-022-04684-3.

Correspondence and requests for materials should be addressed to Shuguo Hou, Ping He or Libo Shan.

Peer review information *Nature* thanks Jian-Min Zhou and the other, anonymous, reviewer(s) for their contribution to the peer review of this work. Peer reviewer reports are available.

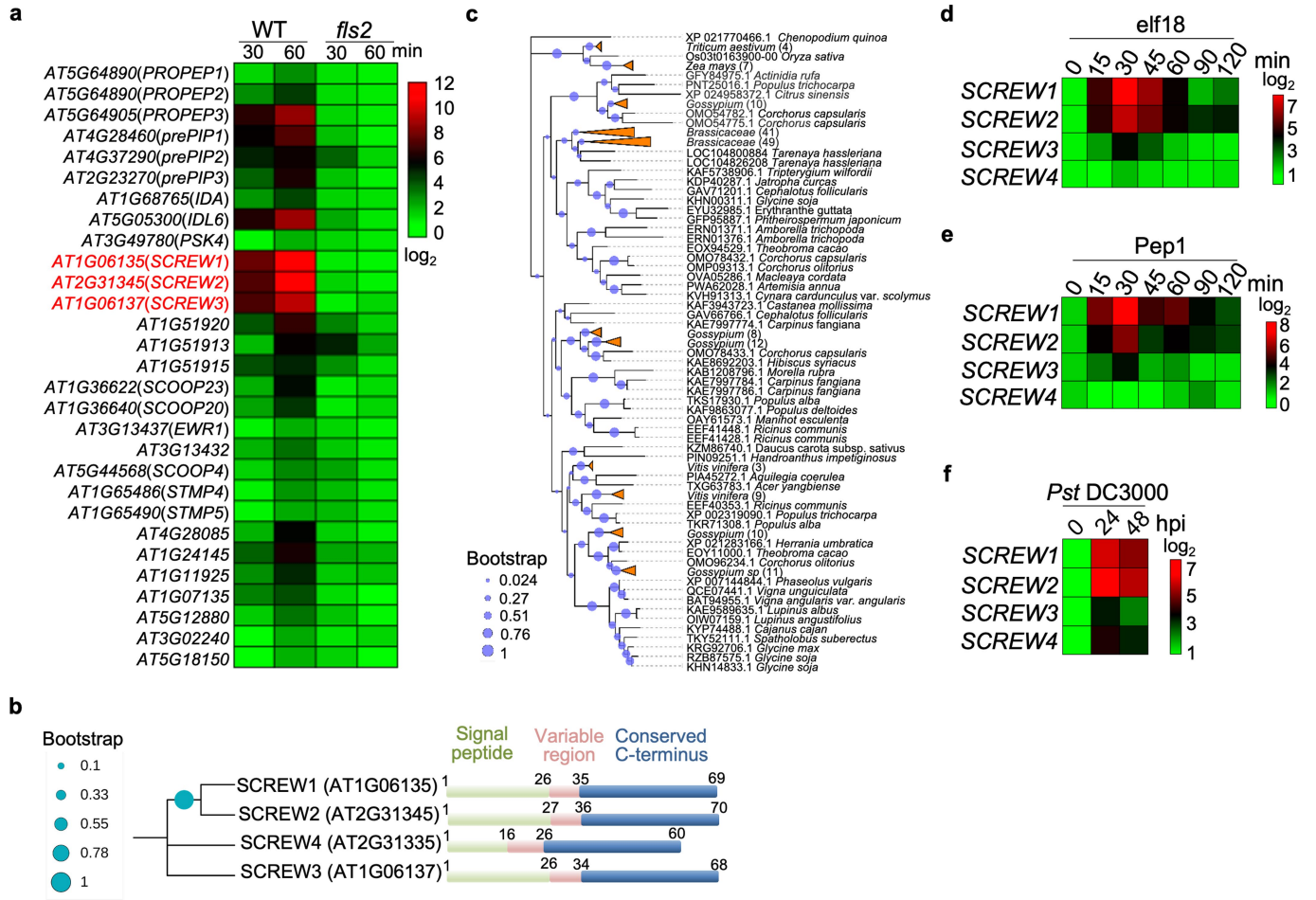

Extended Data Fig. 1 | Identification of SCREWs in *Arabidopsis*. **a**, Upregulation of *Arabidopsis* peptide genes by flg22 in an FLS2-dependent manner. The gene expression data were extracted from an RNA-Seq analysis[17] and subjected to data adjustment by $\log_2$ transformation using TBtools for the heat map. **b**, Phylogenetic analysis of *Arabidopsis* SCREW homologs and schematic diagrams of different domains. The phylogenetic tree was constructed with MEGAX using neighbour-joining methods. The bootstrap values from 1,000 replications are indicated on the branches. **c**, SCREW orthologs are present in dicots and monocots. Protein sequences were blast-searched against the NCBI database, and wheat, rice, and maize genomes using *Arabidopsis* SCREW1 as a query. The phylogenetic tree was constructed as indicated in (**b**) and displayed with iTOL v5 online software (https://itol.embl.de/). The bootstrap values from 1,000 replications are shown on the branches. **d**, *SCREWs* are upregulated after elf18 treatments. Ten-day-old plate-grown seedlings were treated with 200 nM elf18. The expression of *SCREWs* normalized to *UBQ10* was analysed by RT–qPCR. Means ($n = 4$, biologically independent samples) of fold induction shown as $\log_2$ values were used to construct heat map using TBtools. **e**, *SCREWs* are upregulated after Pep1 treatments. Ten-day-old plate-grown seedlings were treated with 200 nM Pep1. The expression of *SCREWs* was detected and shown as in (**d**) ($n = 4$, biologically independent samples). **f**, *SCREWs* are upregulated after *Pst* DC3000 infections. Ten-day-old plate-grown seedlings were treated with *Pst* DC3000 at $OD_{600\,nm} = 0.01$, and gene expression was analysed as in (**d**) ($n = 3$, biologically independent samples).

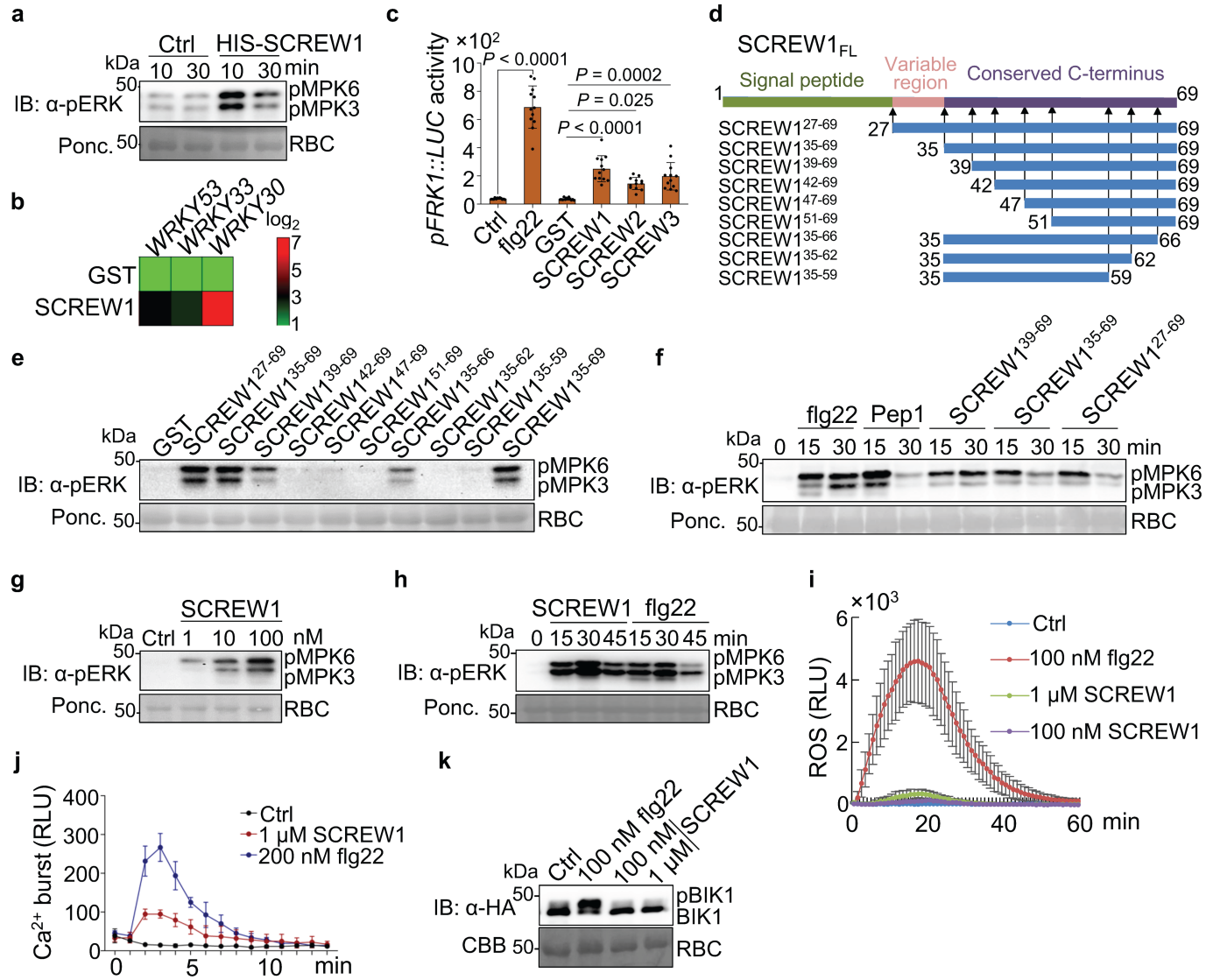

Extended Data Fig. 2 | SCREWs activate PTI responses. a, Recombinant His-SCREW1 induces MAPK activation. Ten-day-old plate-grown seedlings were treated with protein elution buffer (Ctrl) or 1 μM His-SCREW1. MAPK activation was analysed by immunoblotting with anti-pERK1/2 antibodies (top), and protein loading is shown by Ponceau S staining (Ponc.) for RBC (bottom). **b**, SCREW1 upregulates the expression of *WRKY30*, *WRKY33*, and *WRKY53*. Ten-day-old plate-grown seedlings were treated with 1 μM GST or GST-SCREW1 for 1 h, and gene expression was analysed by RT–qPCR. Means ($n = 3$, biologically independent samples) of fold induction shown as $\log_2$ values were used to construct heat map using TBtools. **c**, SCREWs induce *FRK1* promoter activities. Protoplasts were co-transfected with pFRK1::LUC and pUBQ10::GUS followed by treatment with ddH_2O (Ctrl), 100 nM flg22, 1 μM GST, GST-SCREW1, GST-SCREW2, or GST-SCREW3 for 4 h. The *FRK1* promoter activity was presented as the ratio of luciferase to GUS values. Data were analysed by one-way ANOVA followed by Tukey's test, and are shown as mean ± s.d. ($n = 12$, biologically independent samples). *P* values are provided in the graph and Supplementary Table 3. **d**, Schematic diagrams of full-length (FL) and truncated SCREW1 variants. Domains of the signal peptide, variable region, and C-terminal conserved region are shown with aa positions labelled. **e**, SCREW1-induced MAPK activation requires its conserved C-terminus. Ten-day-old seedlings were treated with 1 μM GST or different GST-SCREW1 truncation proteins for 15 min, and the MAPK activation was detected as in (**a**). **f**, Synthesized peptides corresponding to the conserved C-terminal domain in SCREW1 induce MAPK activation. Ten-day-old plate-grown seedlings were incubated with 100 nM flg22, 100 nM Pep1, or 100 nM different SCREW1 variants, and the MAPK activation was detected as in (**a**). **g**, SCREW1 induces MAPK activation at a subnanomolar scale. Ten-day-old plate-grown seedlings were treated with synthesized peptides corresponding to SCREW1$^{39-69}$ with indicated concentrations for 15 min, and MAPK activation was detected as in (**a**). **h**, SCREW1 induces a comparable MAPK activation with flg22. Ten-day-old plate-grown WT seedlings were treated with 500 nM SCREW1 or 100 nM flg22 for the indicated time. **i**, SCREW1 induces a weak ROS burst. Leaf discs from four-week-old soil-grown WT plants were treated with or without 100 nM flg22, 100 nM or 1 μM SCREW1, and ROS production was measured as relative light units (RLU) by a luminometer over 60 min. Data are shown as mean ± s.e.m. ($n = 12$, biologically independent samples). **j**, SCREW1 induces a moderate cytoplasmic Ca^{2+} increase relative to flg22. Protoplasts were transfected with p35S::mCherry-AEQ and incubated for 6 h, followed by treatment with 1 μM SCREW1 or 200 nM flg22. Cytoplasmic Ca^{2+} concentration was detected over 15 min. Data are shown as mean ± s.d. ($n = 3$, biologically independent samples). **k**, SCREW1 does not induce BIK1 phosphorylation. Protoplasts expressing BIK1-HA were treated with 100 nM flg22, 100 nM, or 1 μM SCREW1 for 10 min. BIK1-HA proteins were detected by immunoblotting using anti-HA antibodies (top) with protein loading shown by Coomassie brilliant blue (CBB) staining for RBC (bottom). Experiments were repeated at least three times with similar results.

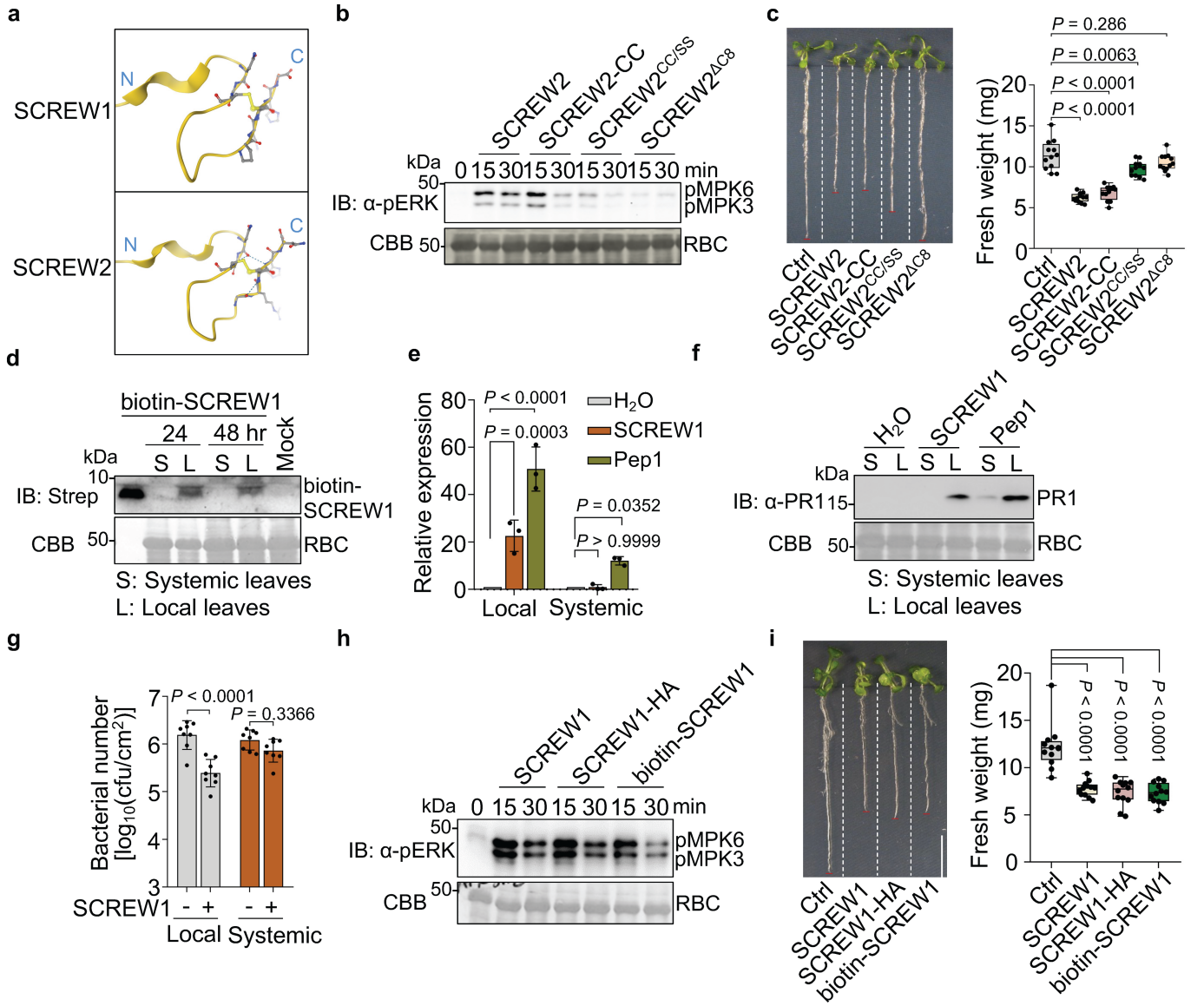

Extended Data Fig. 3 | Two conserved cysteine residues are required for SCREW activities, and SCREW1 is not mobile. a, Predicted structures of SCREW1 and SCREW2 C-terminal 23 aa. Structures were predicted using AlphaFold Protein Structure Database (https://www.alphafold.ebi.ac.uk/). Disulfide bonds are shown by yellow sticks. **b**, Two cysteine residues are required for SCREW2 activation of MAPKs. Ten-day-old plate-grown WT seedlings were treated with or without 100 nM SCREW2, SCREW2(CC), SCREW2(CC/SS) and SCREW2(ΔC8). MAPK activation was analysed by immunoblots with anti-pERK1/2 antibodies (top), and the protein loading is shown by CBB staining for RBC (bottom). **c**, Two cysteine residues are required for SCREW2-induced seedling growth inhibition. Three-day-old plate-grown WT seedlings were transferred into liquid ½MS medium without (Ctrl) or with 1 μM peptides. Images were taken (left), and fresh weights of seedlings (right) were measured seven days later. Data are shown as box plots with the interquartile range as the upper and lower confines, minima and maxima as whiskers, and the median as a solid line ($n = 12$, biologically independent samples). **d**, The biotin-SCREW1 peptide is not mobile. The third pair of true leaves of four-week-old plants were infiltrated with biotin-SCREW1, and both third (local) and fourth (systemic) pairs of true leaves were collected for the detection of biotin-SCREW1 by immunoblotting with HRP-labelled Streptavidin (top). The protein loading control is shown by CBB staining for RBC (bottom). **e**, Local application of SCREW1 does not induce *PR1* expression in distal leaves. The third pair of true leaves from four-week-old plants were infiltrated with H_2O, 500 nM Pep1, or 500 nM SCREW1, and both third (local) and fourth (systemic) pairs of true leaves were collected 24 h later for RT–qPCR using *ACTIN2* as internal controls. Data of induction fold compared to H_2O treatment are shown as mean ± s.d. ($n = 3$, biologically independent samples). **f**, Local application of SCREW1 does not induce PR1 accumulation in distal leaves. The experiment was performed as in **e**, and PR1 proteins were detected by immunoblotting with anti-PR1 antibodies (top). The protein loading control is shown by CBB staining for RBC (bottom). **g**, Local application of SCREW1 does not induce disease resistance in distal leaves. The third pair of leaves were pre-infiltrated with 500 nM SCREW1 followed by *Pst* DC3000 inoculation 24 h later on both third and fourth pairs of leaves. Bacterial growth was detected at three days post-inoculation (dpi). Data are shown as the means ± s.d. ($n = 8$, biologically independent samples). **h**, The biotin-SCREW1 and SCREW1-HA peptides have similar activities with SCREW1 for MAPK activation. Ten-day-old plate-grown WT seedlings were treated with or without 100 nM SCREW1, biotin-SCREW1, and SCREW1-HA. MAPK activation was analysed by immunoblots using anti-pERK1/2 antibodies (top) with the protein loading shown by CBB staining for RBC (bottom). **i**, The biotin-SCREW1 and SCREW1-HA peptides have similar activities with SCREW1 for seedling growth inhibition. The experiment was performed as in (**c**). Data are shown as box plots with the interquartile range as the upper and lower confines, minima and maxima as whiskers, and the median as a solid line ($n = 12$, biologically independent samples). Experiments were repeated three times with similar results. Data were analysed by one-way (**c**, **i**), or two-way (**e**, **g**) ANOVA followed by Tukey's test. Exact *P* values are provided in the graphs and Supplementary Table 3.

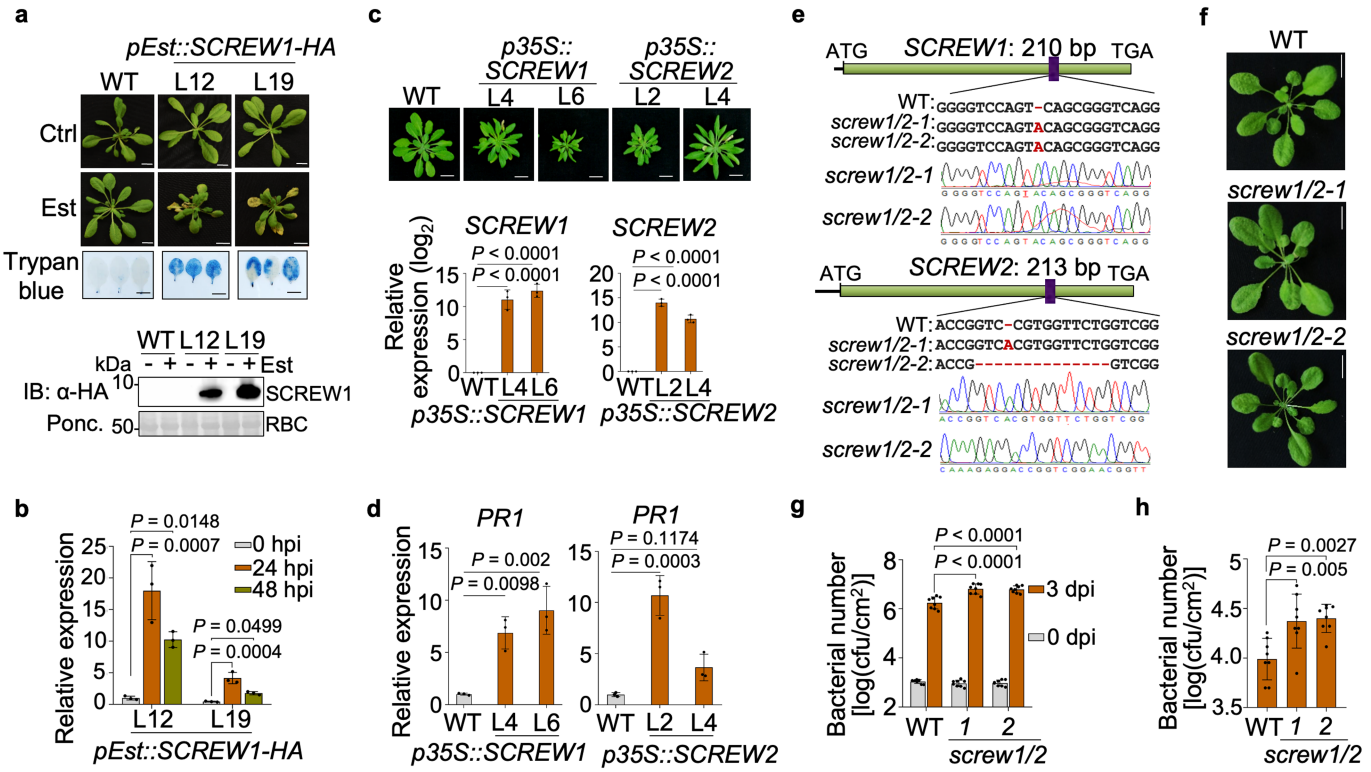

Extended Data Fig. 4 | SCREW1 and SCREW2 are involved in plant immunity. **a**, Inducible overexpression of *SCREW1* leads to leaf chlorosis. Four-week-old transgenic plants carrying pEst::SCREW1-HA in WT (L12 & L19) were sprayed with 0.05% DMSO (Ctrl) or 50 μM β-oestradiol (Est), and then imaged five days later (Scale bar, 1 cm) with trypan blue staining (Scale bar, 0.5 cm). SCREW1-HA proteins were detected by immunoblots with anti-HA antibodies (bottom). **b**, SCREW1 overexpression elevates *PR1* expression. Four-week-old soil-grown pEst::SCREW1-HA transgenic plants were sprayed with 50 μM β-oestradiol. The *PR1* expression normalized to *ACTIN2* was analysed by RT–qPCR. Data are shown as mean ± s.d. ($n = 3$, biologically independent samples). **c**, Overexpression of *SCREW1* or *SCREW2* leads to plant growth retardation and leaf curling. Transgenic lines carrying p35S::SCREW1 or p35S::SCREW2 were grown on soil for five weeks before photography. Scale bar, 1 cm. The expression of *SCREWs* normalized to *ACTIN2* in ten-day-old plate-grown seedlings was analysed with RT–qPCR. Data are shown as mean ± s.d. ($n = 3$, biologically independent samples). **d**, Overexpression of *SCREW1* or *SCREW2* upregulates *PR1* expression. Relative *PR1* expression levels normalized to *UBQ10* in four-week-old soil-grown plants were analysed with RT–qPCR. Data are shown as mean ± s.d. ($n = 3$, biologically independent samples). **e**, CRISPR/Cas9-mediated gene editing of *SCREW1* and *SCREW2*. Mutations of *SCREW1* and *SCREW2* in *screw1/2-1* and *screw1/2-2* were detected by DNA sequencing and shown as chromatographs. Two homozygous lines, *screw1/2-1* and *screw1/2-2*, carry the same nucleotide insertion in *SCREW1* for both lines, and a nucleotide insertion and a sixteen-nucleotide deletion in *SCREW2* for *screw1/2-1* and *screw1/2-2*, respectively. **f**, The *screw1/2* mutants are morphologically indistinguishable from WT plants. Plants were grown on soil for four weeks and photographed. Scale bar, 1 cm. **g**, The *screw1/2* mutants are more susceptible to *Pst* DC3000. Leaves of four-week-old WT and *screw1/2* mutant lines (1 & 2) were hand-inoculated with *Pst* DC3000 at $OD_{600\,nm} = 5 \times 10^{-4}$. Bacterial numbers were measured at 0 and 3 dpi and shown as mean ± s.d. ($n = 8$, biologically independent samples). **h**, The *screw1/2* mutants show enhanced susceptibility to *Pst* DC3000 *hrcC*$^-$. Leaves of four-week-old soil-grown WT and *screw1/2* mutant lines (1 & 2) were hand-inoculated with *Pst* DC3000 *hrcC*$^-$ at $OD_{600\,nm} = 0.005$, and the bacterial number was measured at 3 dpi. Data are shown as mean ± s.d. ($n = 8$, biologically independent samples). Experiments were repeated at least three times with similar results. Data were analysed by one-way (**b**-**d**, **h**) or two-way (**g**) ANOVA followed by Tukey's test. Exact *P* values are provided in the graphs and Supplementary Table 3.

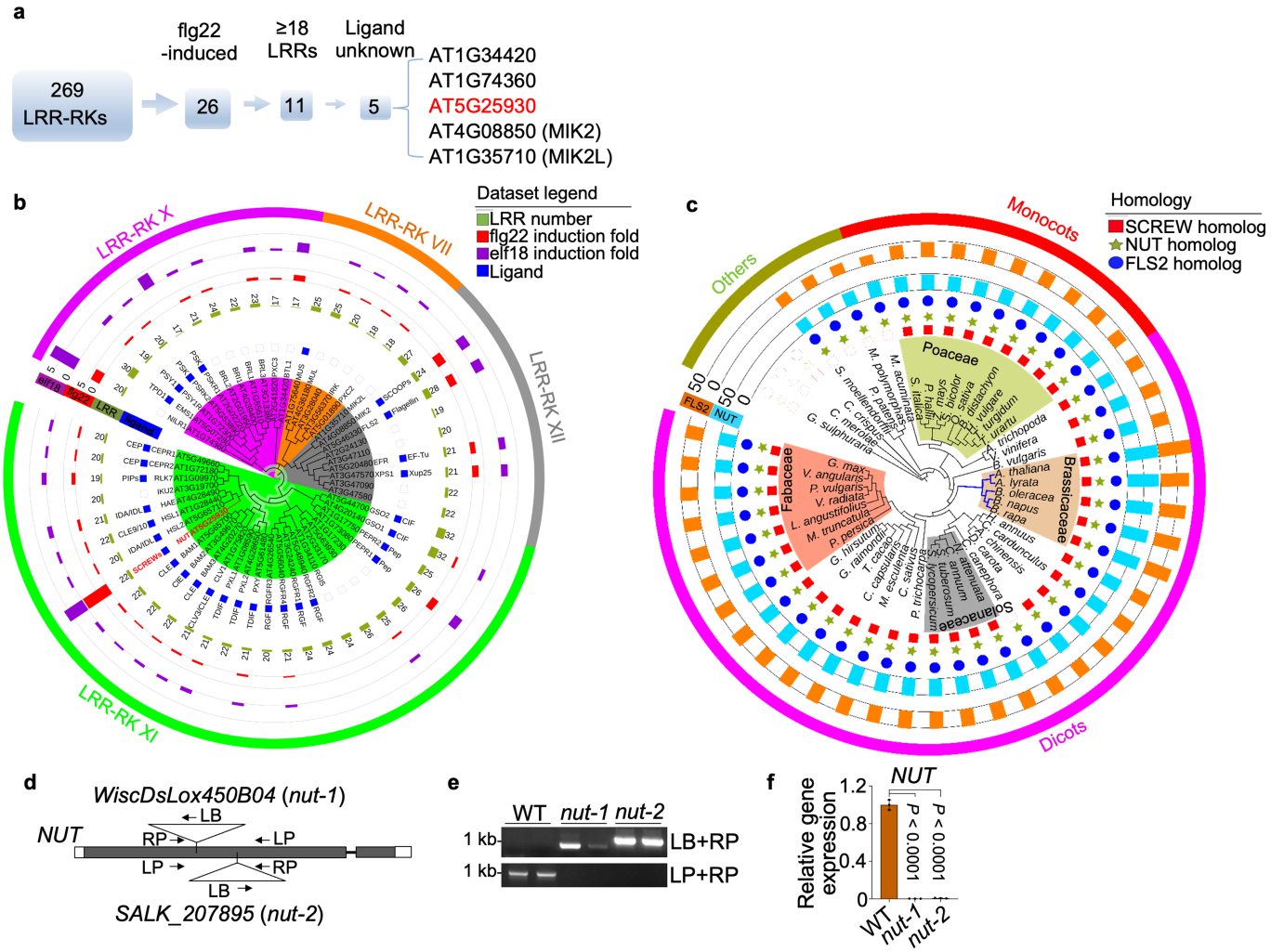

Extended Data Fig. 5 | Identification of the SCREW receptor NUT. a, Scheme to identify SCREW receptor candidates. Among 269 LRR-RKs in *Arabidopsis*, 26 members are upregulated by flg22 treatment, among which 11 members contain at least 18 LRRs in the extracellular domain. The cognate ligands of five of them remain unknown at the time of the study. **b**, NUT belongs to the XI subfamily of LRR-RK and is phylogenetically close to HAE and HSLs. Phylogenetic analysis of 52 LRR-RKs from the subfamily VII (orange curved line), X (purple curved line), XI (green curved line), and XII (grey curved line) is shown. Purple and red bars indicate the induction folds after elf18 and flg22 treatments, respectively. Olive green bars with numbers indicate the number of LRRs. Blue squares indicate cognate ligands of LRR-RKs. AT5G25930 (NUT) is highlighted in bold red font. The protein sequences were retrieved from NCBI (https://www.ncbi.nlm.nih.gov/) for MEGAX phylogenetic analysis using the neighbour-joining method with 1,000 bootstrap replicates. The phylogenetic tree was displayed by iTOL (https://itol.embl.de/). The expression data were from GENEVESTIGATOR V3. **c**, SCREWs and NUT are conserved in dicots and monocots. Protein sequences were blast-searched in NCBI using *Arabidopsis* SCREW1, NUT, or FLS2 as queries, and the phylogenetic analysis was performed as in (**b**). Red, purple, and olive curved lines indicate monocots, dicots, and other plant classes, respectively; Orange and teal bars indicate the percentage of homology of FLS2 and NUT in different plant species, respectively. Blue dots, olive stars, and red squares indicate FLS2, NUT, and SCREW homologs, respectively. Peach, lime green, grey, and brown fans denote different plant families. **d**, Diagram of *AT5G25930* (*NUT*) with annotated T-DNA insertion sites in *nut-1* (*WiscDslox450B04*) and *nut-2* (*SALK_207895*). Solid bars indicate exons, lines for introns, and open boxes for UTRs. Arrows indicate primers used for genotyping. **e**, Genotyping of *nut-1* and *nut-2*. The T-DNA insertions in the *NUT* coding region were PCR-amplified using genomic DNAs of WT, *nut-1*, or *nut-2* as templates and primers shown in (**d**). **f**, RT–qPCR analysis of *NUT* transcripts. *NUT* expression levels in ten-day-old plate-grown seedlings were analysed using RT–qPCR with *UBQ10* as an internal control. Data are shown as mean ± s.d. ($n = 3$, biologically independent samples) with one-way ANOVA followed by Tukey's test. Exact *P* values are provided in the graph and Supplementary Table 3. Experiments were repeated three times with similar results (**e**, **f**).

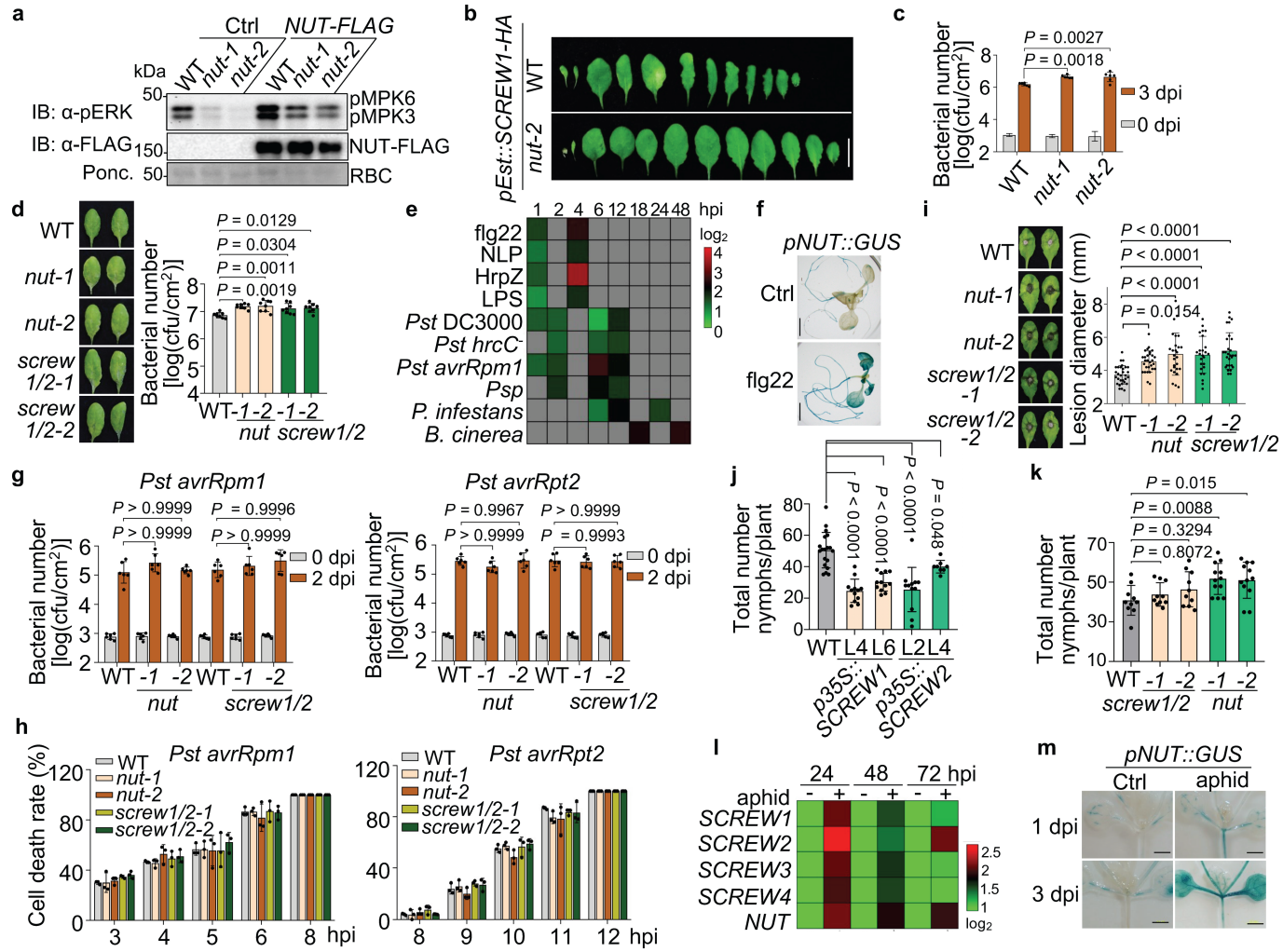

Extended Data Fig. 6 | See next page for caption.

Extended Data Fig. 6 | NUT is required for SCREW-triggered responses and resistance to *B. cinerea* and green peach aphids. a, *NUT-Flag* restores SCREW1-induced MAPK activation in *nut* protoplasts. Protoplasts were transfected with an empty vector (Ctrl) or *NUT-Flag* followed by treatment with 100 nM SCREW1 for 15 min. MAPK activation and NUT-Flag proteins were detected with anti-pERK1/2 (top) and anti-Flag antibodies (middle), respectively. Protein loading is shown by Ponceau S staining (Ponc.) for RBC (bottom). **b**, Inducible overexpressing SCREW1-triggered leaf chlorosis is blocked in *nut-2*. Five-week-old pEst::SCREW1-HA transgenic plants in WT and *nut-2* were sprayed with 50 μM β-oestradiol and photographed five days later. Scale bar, 1cm. **c**, The *nut* mutants are more susceptible to *Pst* DC3000 than WT. Leaves of four-week-old plants were hand-inoculated with *Pst* DC3000 at $OD_{600\,nm} = 5 \times 10^{-4}$. The bacterial numbers were measured at 0 and 3 dpi. Data are shown as mean ± s.d. ($n = 6$, biologically independent samples). **d**, The *nut* and *screw1/2* mutants are more susceptible to spray-inoculated *Pst* DC3000. Four-week-old plants were sprayed with *Pst* DC3000 at $OD_{600\,nm} = 0.2$. The disease symptoms and bacterial numbers were determined at 72 hpi. Data are shown as mean ± s.d. ($n = 8$, biologically independent samples). **e**, *NUT* is upregulated by MAMPs and pathogens. Data were retrieved from the *Arabidopsis* eFP browser (http://bar.utoronto.ca/efp/cgi-bin/efpWeb.cgi) and shown as histograms. Grey squares indicate no data available from eFP browser. Flg22, NLP, HrpZ, and lipopolysaccharide (LPS) are MAMPs. *Pst* DC3000, *Pst* DC3000 *hrcC*$^-$, *Pst* DC3000 *avrRpm1* and *P. syringae* pv. *phaseolicola* (*Psp*) are bacterial pathogens. *Phytophthora infestans* is an oomycete, and *B. cinerea* is a fungal pathogen. **f**, Flg22 upregulates *NUT* promoter activities. Two-week-old plate-grown pNUT::GUS/WT transgenic seedlings were treated without (Ctrl) or with 100 nM flg22 for 2 h, followed by GUS staining and microscopic imaging under a stereomicroscope. Scale bar, 2 mm. **g**, The *nut* and *screw1*/2 mutants do not affect plant resistance to *Pst* DC3000 *avrRpm1* (left) and *Pst* DC3000 *avrRpt2* (right). Bacteria were infiltrated into four-week-old plant leaves at $OD_{600\,nm} = 0.001$, and bacterial populations were determined at 2 dpi. Data are shown as mean ± s.d. ($n = 6$, biologically independent samples). **h**, The *nut* and *screw1*/2 mutants do not affect plant HR to *Pst* DC3000 *avrRpm1* (left) and *Pst* DC3000 *avrRpt2* (right). Bacteria were infiltrated into four-week-old plant leaves at $OD_{600\,nm} = 0.08$, and wilting leaves were counted at the indicated time points. At least 20 leaves were inoculated for each genotype and inoculum. The cell death rate was presented as the ratio of wilting leaves to total inoculated leaves. Data are shown as mean ± s.d. ($n = 3$, biologically independent samples). **i**, The *nut* and *screw1/2* mutants are more susceptible to *B. cinerea*. Detached leaves of four-week-old plants were drop-inoculated with *B. cinerea* at 10^7 spores/mL. Disease phenotype was recorded at 48 hpi. Data are shown as mean ± s.d. (left to right: $n = 30, 29, 27, 25, 28$, biologically independent samples). **j**, The p35S::SCREW1 and p35S::SCREW2 plants show enhanced resistance to aphids. Six-age-synchronized second instar nymphs of *Myzus persicae* were inoculated onto leaves of four-week-old plants. The number of neonates per plant (n) was counted at 10 dpi. Data are shown as mean ± s.d. (left to right: $n = 19, 12, 12, 12, 8$, biologically independent samples). **k**, The *nut* mutants are more susceptible to aphid infections than WT plants. The experiments and statistics were performed as in **j** (left to right: $n = 10, 10, 10, 12, 12$, biologically independent samples). **l**, The expression of *SCREWs* and *NUT* is induced by aphid infections. Leaves of two-week-old plants were inoculated with or without aphid nymphs for 24, 48, and 72 h. The expression of *SCREWs* and *NUT* normalized to *UBQ10* was analysed by RT–qPCR. Means ($n = 3$, biologically independent samples) of fold induction compared to non-treatment are shown as $\log_2$ transformation to construct heat map using TBtools. **m**, The *NUT* promoter activity is induced by aphid infections. Two-week-old soil-grown transgenic plants carrying pNUT::GUS were inoculated with aphid nymphs and subjected to GUS staining at 1 and 3 dpi. The pictures were taken under a stereomicroscope. Scale bar, 2 mm. Experiments except **e** were repeated three times with similar results. Data were analysed by one-way (**d**, **i**) or two-way (**c**, **g**) ANOVA followed by Tukey's test, or one-way ANOVA followed by Dunnett's test (**j**, **k**). Exact *P* values are provided in the graphs and Supplementary Table 3.

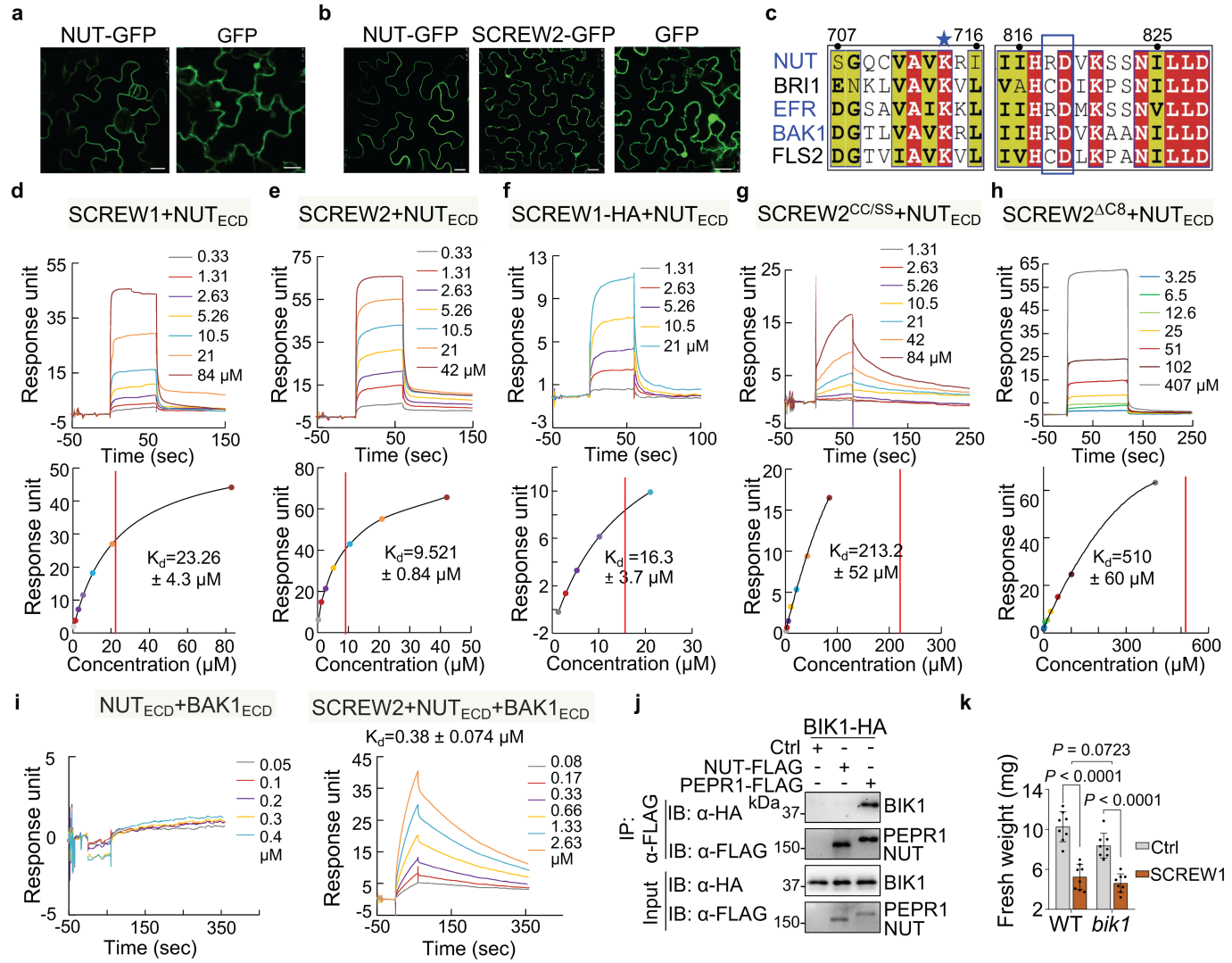

Extended Data Fig. 7 | SPR assays of SCREW and SCREW derivatives binding to NUT$_{ECD}$, and *bik1* does not affect SCREW1-induced inhibition of seedling growth. a, NUT-GFP is localized on the plasma membrane. Transgenic seedlings carrying p35S::GFP or p35S::NUT-GFP were grown on ½MS plates for seven days, and true leaves were imaged using a confocal laser scanning microscopy. Scale bar, 25 μm. **b**, NUT-GFP and SCREW2-GFP are localized on the plasma membrane in *N. benthamiana*. *N. benthamiana* leaves were infiltrated with *A. tumefaciens* GV3101 carrying p35S::NUT-GFP, p35S::SCREW2-GFP or p35S::GFP and imaged under a confocal microscope at 3 dpi. Scale bar, 25 μm. **c**, Sequence alignment of parts of cytosolic kinase domains of different RKs, including NUT, FLS2, BAK1, EFR, and BRI1. The sequences were aligned by MEGAX and visualized with ESPript 3.0 (http://espript.ibcp.fr/). The lysine (K) required for ATP-binding (blue asterisk) and the RD/non-RD motif (blue rectangle) were marked. The positions of amino acids in NUT were labelled on the top. **d**-**g**, SPR assays of SCREW1 (**d**), SCREW2 (**e**), SCREW1-HA (**f**), SCREW2$^{CC/SS}$ (**g**) binding to NUT$_{ECD}$ under pH 5.7. NUT$_{ECD}$ was immobilized on a sensor chip, and synthesized SCREW peptides were used as flow-through analytes. The top panel shows the SPR sensorgram profile of SCREW peptides at gradient concentrations flowing through the NUT$_{ECD}$-immobilized chip. The bottom panel shows the steady-state affinity (binding at equilibrium) with different K_d. **h**, The C-terminus of SCREW2 is essential for its binding to NUT$_{ECD}$. The SPR assays were performed as in Fig. 3f, g. **i**, BAK1 promotes the SCREW2-NUT binding affinity. (Left) SPR detection of BAK1$_{ECD}$ binding to NUT$_{ECD}$ in the absence of SCREW peptides. BAK1$_{ECD}$ was used as flow-through analytes on a sensor chip immobilized with NUT$_{ECD}$. At the concentration tested, no binding between NUT$_{ECD}$ and BAK1$_{ECD}$ was detected. (Right) SPR detection of SCREW2 binding to NUT$_{ECD}$ in the presence of BAK1$_{ECD}$. NUT$_{ECD}$ was immobilized on a sensor chip, and SCREW2 peptides at gradient concentrations together with 0.1 μM BAK1$_{ECD}$ proteins were used as flow-through analytes. The K_d of SCREW2 binding to NUT$_{ECD}$ in the presence of BAK1 is 0.38 ± 0.074 μM. The SPR assays were performed at pH 5.7. **j**, NUT does not associate with BIK1. Protoplasts were co-transfected with BIK1-HA and NUT-Flag, PEPR1-Flag, or a control vector (Ctrl). Total proteins were immunoprecipitated with anti-Flag agarose beads and detected with anti-HA or anti-Flag antibodies (top two). Proteins before immunoprecipitation (IP) are shown as input controls (bottom two). **k**, SCREW1 inhibits seedling growth in the *bik1* mutant. Three-day-old plate-grown seedlings were transferred into liquid ½MS medium with or without 1 μM SCREW1 and grown for seven days. Fresh weights of seedlings are shown as as mean ± s.d. (n = 8, biologically independent samples). Data were analysed by two-sided Student's t-test and two-way ANOVA followed by Tukey's test. P values are provided in the graph and Supplementary Table 3. Experiments were repeated twice (**a**, **b**, **d**–**i**) or three times (**j**, **k**) with similar results.

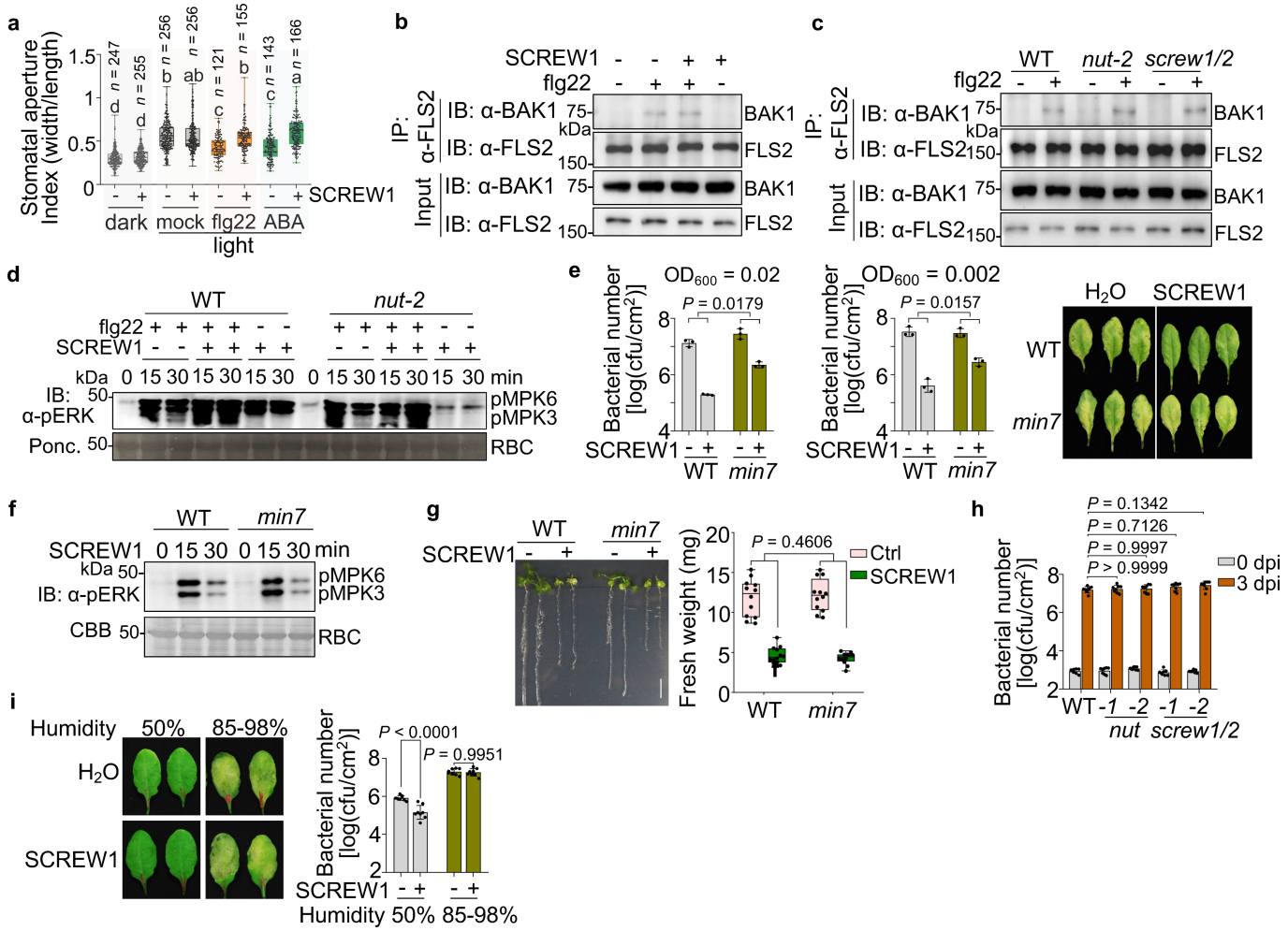

Extended Data Fig. 8 | SCREW–NUT does not affect flg22-triggered early signalling events but partially requires MIN7. a, SCREW1 suppresses flg22- or ABA-induced stomatal closure. The stomatal apertures were measured after treatment without or with 1 μM SCREW1, 1 μM flg22, 10 μM ABA, or a combination of SCREW1 with flg22 or ABA for 2 h under the light. Data are shown as box plots with the interquartile range as the upper and lower confines, minima and maxima as whiskers, and the median as a solid line. Different letters denote a statistically significant difference ($P < 0.05$). n = number of stomata in the graph. **b**, SCREW1 does not affect the flg22-induced FLS2-BAK1 association. Four-day-old plate-grown WT seedlings were transferred into liquid ½MS for six days, followed by 100 nM flg22, 100 nM SCREW, or a combination of 100 nM flg22 and 100 nM SCREW for 10 min. Proteins were subjected for IP assays using anti-FLS2 antibodies and followed by immunoblotting using anti-BAK1 or anti-FLS2 antibodies. Top two panels show the IPed products, and bottom two panels show protein inputs. **c**, The *nut* and *screw* mutants do not affect the flg22-induced FLS2-BAK1 association. Four-day-old plate-grown seedlings were transferred into liquid ½MS for six days, followed by 100 nM flg22 for 10 min. Co-IP analysis was similar to the above in **b**. **d**, SCREW1 and NUT do not affect flg22-induced MAPK activation. Ten-day-old seedlings were treated with 100 nM flg22, 100 nM SCREW1, or a combination of 100 nM flg22 and 100 nM SCREW1. MAPK activation was analysed by immunoblotting with anti-pERK1/2 antibodies (top), and protein loading is shown by Ponceau S staining (Ponc.) for RBC (bottom). **e**, SCREW1-triggered resistance to *Pst* DC3000 is partially abolished in *min7*. Four-week-old plants were pre-infiltrated with 0.5 μM SCREW1, or H_2O as a control. After 24 h, *Pst* DC3000 was infiltrated at a concentration of $OD_{600\,nm}$ = 0.02 or 0.002, and bacterial counting was performed at 1 dpi for $OD_{600\,nm}$ = 0.02, and 2 dpi for $OD_{600\,nm}$ = 0.002. Data are shown as means ± s.d. (n = 3, biologically independent samples) (left). The picture was taken at 3 dpi with $OD_{600\,nm}$ = 0.002 (right). **f**, MIN7 is not required for SCREW1 activation of MAPKs. Ten-day-old plate-grown seedlings were treated with 100 nM SCREW1. MAPK activation was analysed by immunoblots with anti-pERK1/2 antibodies (top), and the protein loading is shown by CBB staining for RBC (bottom). **g**, MIN7 is not required for SCREW1 suppression of seedling growth. Three-day-old plate-grown seedlings were transferred into liquid ½MS medium with or without 1 μM SCREW1. Seedlings were imaged (left) and weighed (right) seven days post-treatment. Scale bar, 1 cm. Fresh weights of seedlings are shown as box plots with the interquartile range as the upper and lower confines, minima and maxima as whiskers, and the median as a solid line (n = 12, biologically independent samples). **h**, The susceptibility of *nut* and *screw1/2* mutants to *Pst* DC3000 is comparable to WT plants under high humidity with transient apoplast water supplementation. Leaves of four-week-old plants were inoculated with *Pst* DC3000 at $OD_{600\,nm} = 1 \times 10^{-4}$ and kept under 85–98% humidity for three days before bacterial counting. Transient water supplementation (+H_2O) was performed by keeping plants under high humidity after syringe-infiltration without air-drying inoculated leaves as described previously[32]. Data are shown as means ± s.d. (n = 8, biologically independent samples). **i**, SCREW1-triggered plant resistance to *Pst* DC3000 is compromised under high humidity with transient apoplast water supplementation. Leaves of four-week-old WT plants were pre-infiltrated with H_2O (Ctrl) or 1 μM SCREW1 for 24 h followed by *Pst* DC3000 inoculation. Plants were kept under 50% or 85–98% humidity for three days before bacterial counting. Data are shown as means ± s.d. (n = 8, biologically independent samples). Experiments were repeated three times with similar results. Data were analysed by two-sided Student's t-test (**e**, **g**), one-way (**a**) or two-way (**h**, **i**) ANOVA followed by Tukey's test. Exact P values are provided in the graphs and Supplementary Table 3.

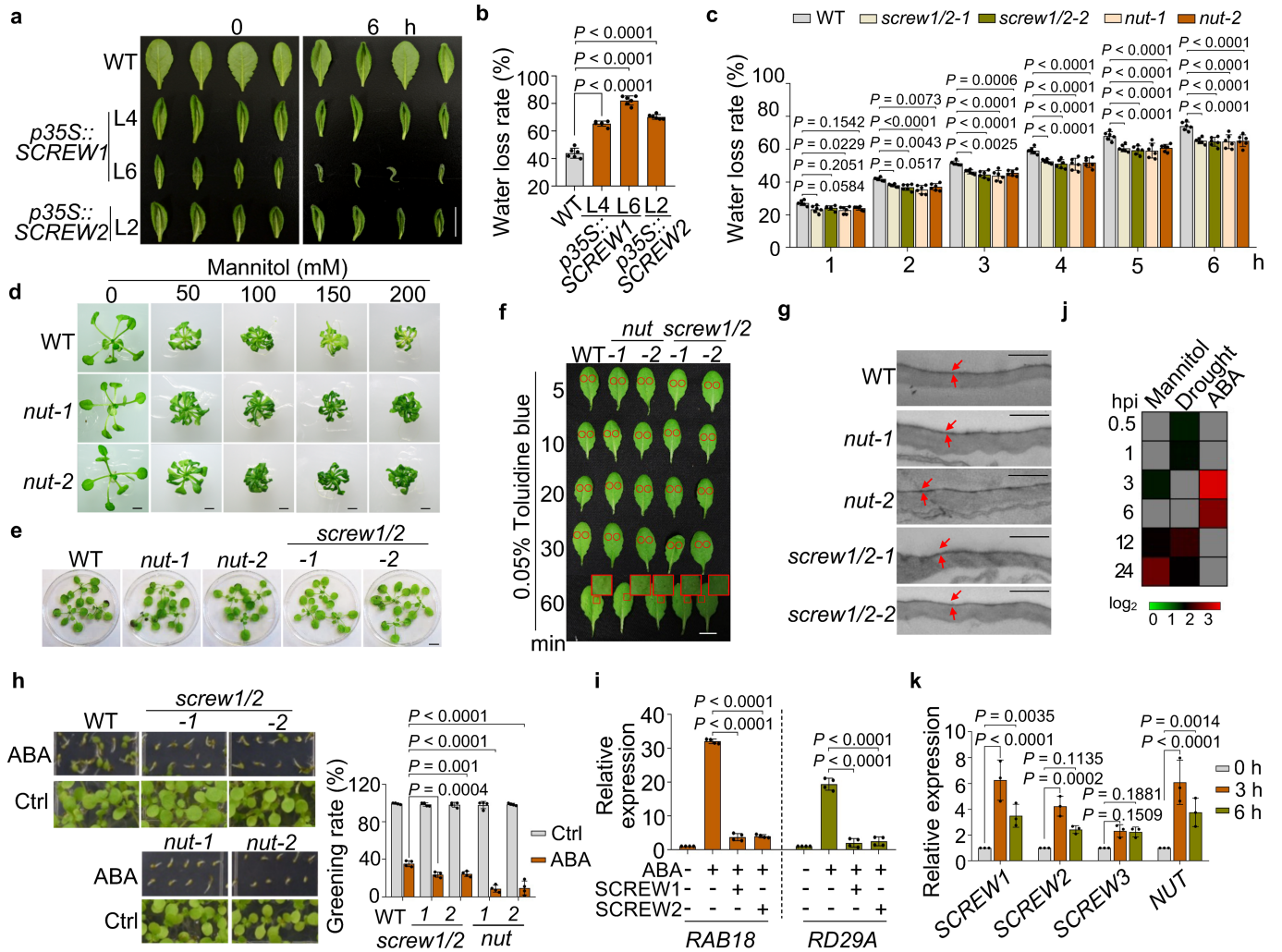

Extended Data Fig. 9 | SCREW–NUT regulates leaf water loss and ABA responses. a, Transgenic plants carrying p35S::SCREW1 or p35S::SCREW2 exhibit curled leaves and increased sensitivity to dehydration stress. Leaves of five-week-old soil-grown plants were detached and imaged at 0 and 6 h after detachment. Scale bar, 1 cm. **b**, Increased water-loss rate in transgenic plants carrying p35S::SCREW1 or p35S::SCREW2. The rates of cumulative water loss from rosette leaves of five-week-old plants were measured at 6 h post-detachment. Data are shown as means ± s.d. ($n = 6$, biologically independent samples). **c**, Reduced water-loss rate in *nut* and *screw1/2*. The rate of cumulative water loss from detached leaves of four-week-old plants was measured at the indicated time points after detachment. Data are shown as means ± s.d. ($n = 6$, biologically independent samples). **d**, Enhanced resistance to mannitol treatment in *nut* mutants. Seedlings were grown on $^1/_2$MS plates with 0, 50, 100, 150, or 200 mM mannitol for 15 days. Scale bar, 2 mm. **e**, Cuticle permeability of *nut* and *screw1/2* seedlings is similar to that of WT. Three-week-old plate-grown plants were soaked with 0.05% toluidine blue for 15 min and washed with ddH_2O before imaging. Scale bar, 1 cm. At least six seedlings for each genotype were analysed for the presence of the blue-coloured patches, which indicate an increased permeability of the stain into the leaf through the cuticle. No apparent differences were observed between WT and mutants. **f**, Leaf cuticle permeability of *nut* and *screw1/2* is similar to that of WT. Leaves of four-week-old soil-grown plants were drop-stained with 0.05% toluidine blue on the adaxial surface for the indicated time. The red circles and rectangles indicate the sites of inoculation. Inserts show zoomed-in areas. No blue-coloured patches were observed, indicating the intact cuticle for each genotype. Scale bar, 20 µm. Scale bar, 1 cm. Ten leaves for each genotype were analysed. **g**, Leaf cuticle layers of *nut* and *screw1/2* are similar to those of WT. Three-week-old plate-grown plant leaves were examined by transmission electron microscopy from the adaxial side. Red arrows indicate cuticles observed as a thin (~80–100 nm) electron-dense layer on the surface of the cell wall. Scale bar, 1 µM. Four leaves of each genotype were analysed. No apparent differences in thickness were detected among different genotypes. **h**, The *nut* and *screw1/2* mutants are more sensitive to ABA treatment than WT plants. Seedlings were grown on $^1/_2$MS plates without (Ctrl) or with 1 µM ABA for seven days (left). Cotyledon greening rates are shown as means ± s.d. (right, $n = 4$, biologically independent repeats). **i**, SCREW1 and SCREW2 suppress ABA-induced expression of *RAB18* and *RD29A* in plants. Ten-day-old plate-grown WT seedlings were treated with H_2O, 10 µM ABA, or combinations of 10 µM ABA and 1 µM SCREW1 or SCREW2 for 3 h. Transcript levels of *RAB18* and *RD29A* normalized to *UBQ10* were determined via RT–qPCR. Data are shown as mean ± s.d. ($n = 4$, biologically independent samples). **j**, *NUT* is upregulated by ABA, mannitol, and drought treatments. The expression data were extracted from Genevestigator V3 and shown as histograms. Grey squares indicate no data available. **k**, *SCREWs* and *NUT* are up-regulated after ABA treatments. Ten-day-old plate-grown WT seedlings were treated with 100 µM ABA for 0, 3, and 6 h. Transcript levels of *SCREWs* and *NUT* normalized to *UBQ10* were determined via RT–qPCR. Data are shown as mean ± s.d. ($n = 3$, biologically independent samples). Experiments were repeated three times with similar results. Data were analysed by one-way (**b**) or two-way (**c**, **h**, **i**, **k**) ANOVA followed by Tukey's test. Exact *P* values are provided in the graphs and Supplementary Table 3.

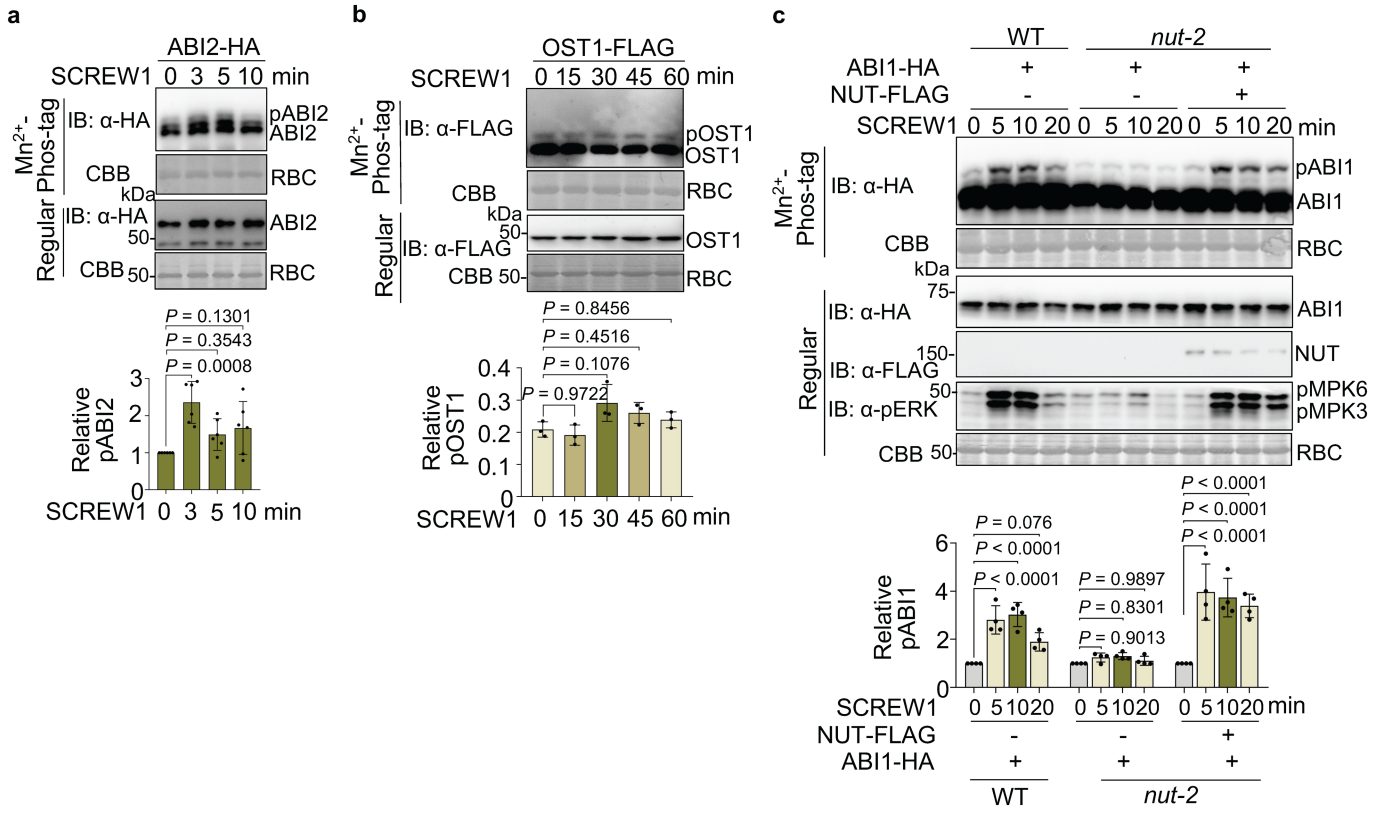

Extended Data Fig. 10 | SCREW1 induces NUT-dependent ABI phosphorylation. a, SCREW1 induces ABI2 phosphorylation. Protoplasts were transfected with *ABI2-HA* followed by treatment with 1 μM SCREW1 for the indicated time. Proteins were separated with Mn^{2+}-Phos-tag (top two) or regular SDS-PAGE (middle two) and detected with anti-HA antibodies. The protein loading is shown by CBB staining for RBC. Signal intensities of the top two bands corresponding to the phosphorylated ABI2 (pABI2) normalized to the input ABI2 in the regular SDS-PAGE from six independent immunoblots were quantified by ImageJ (bottom). The phosphorylation of ABI2 without SCREW1 treatment was set as 1. Data are shown as mean ± s.d. ($n = 6$, biologically independent repeats). **b**, SCREW1 does not induce OST1 phosphorylation. Protoplasts were transfected with *OST1-Flag*, followed by treatment with 1 μM SCREW1 for the indicated time. Proteins were separated with Mn^{2+}-Phos-tag (top two) or regular SDS-PAGE (middle two) and detected with anti-Flag antibodies. The protein loading is shown by CBB staining for RBC. Signal intensities of bands from three independent immunoblots were analysed by ImageJ (bottom). The relative phosphorylation of OST1 represents the ratio of phosphorylated to unphosphorylated OST1. Data are shown as mean ± s.d. ($n = 3$, biologically independent repeats). **c**, SCREW1 induces NUT-dependent ABI1 phosphorylation. Protoplasts were co-transfected with *ABI1-HA* and *NUT-Flag* or a control vector followed by treatment with 1 μM SCREW1 for the indicated time. Proteins were separated by SDS-PAGE with (top two) or without Mn^{2+}-Phos-tag (middle four) and detected with anti-HA or anti-ERK1/2 antibodies. The protein loading is shown by CBB staining for RBC. Signal intensities of bands corresponding to phosphorylated ABI1 (pABI1) normalized to the input ABI1 in the regular SDS-PAGE from four independent immunoblots were quantified by ImageJ (bottom). The phosphorylation of ABI1 without SCREW1 treatment was set as 1. Data are shown as mean ± s.d. ($n = 4$, biologically independent repeats). Experiments were repeated three times with similar results. Data were analysed by one-way (**a**, **b**) or two-way (**c**) ANOVA followed by Tukey's test. Exact *P* values are provided in graphs and Supplementary Table 3.

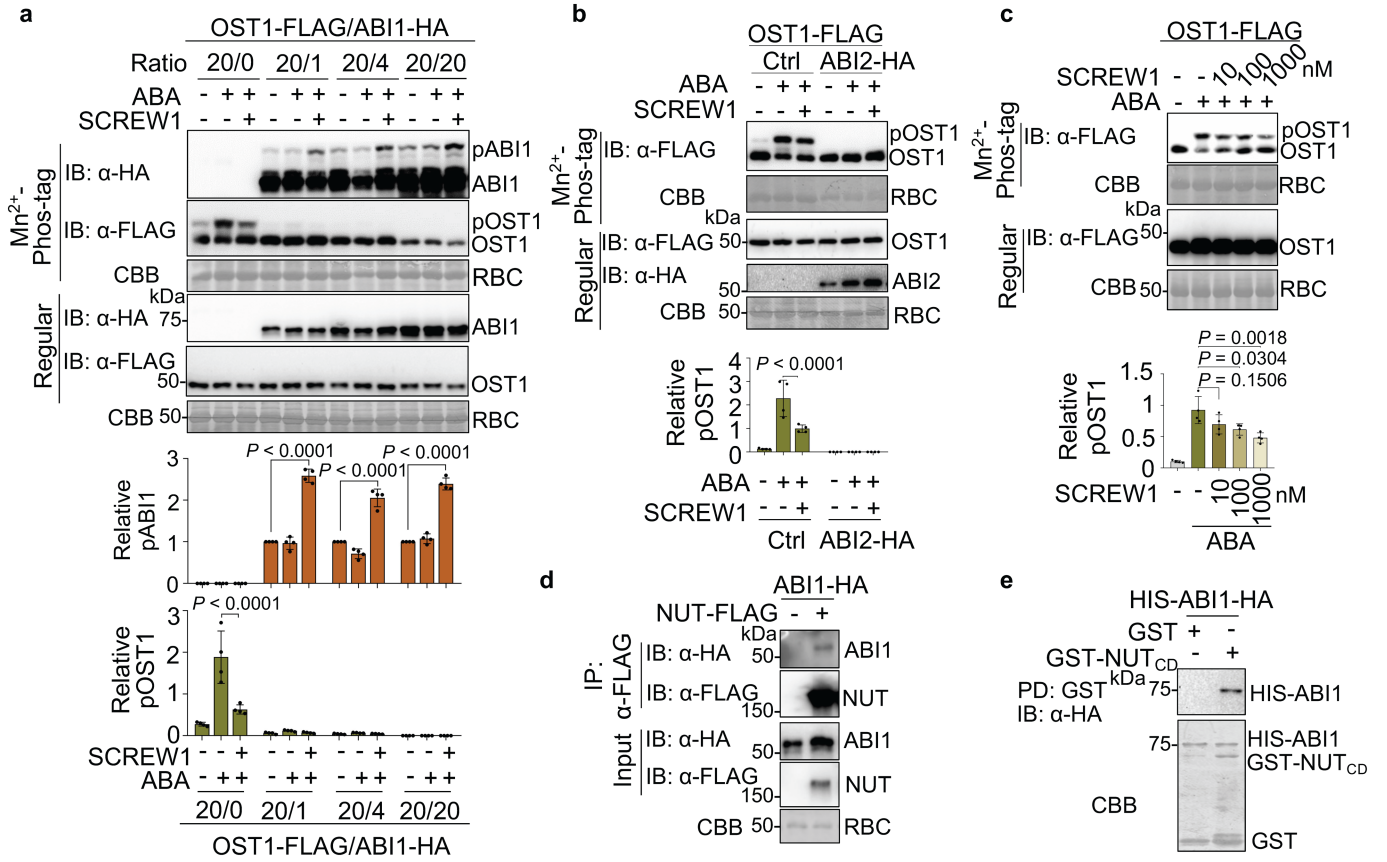

Extended Data Fig. 11 | SCREW1 and ABI suppress ABA-induced OST1 phosphorylation. a, ABI1 suppresses ABA-induced OST1 phosphorylation. Protoplasts were co-transfected with *OST1-Flag* and *ABI1-HA* with the indicated ratio of DNAs, followed by treatment with 1 μM SCREW1 for 5 min before adding 1 μM ABA for an additional 5 min. Proteins were separated with Mn^{2+}-Phos-tag (top three) or regular SDS-PAGE (middle two) and detected with anti-HA or anti-Flag antibodies. The protein loading is shown by CBB staining for RBC. Signal intensities of bands corresponding to phosphorylated ABI1 (pABI1) and OST1 (pOST1) from four independent immunoblots were quantified by ImageJ (bottom two). The relative phosphorylation of OST1 represents the ratio of phosphorylated to unphosphorylated OST1. The phosphorylation of ABI1 without treatment was set as 1. Data are shown as mean ± s.d. ($n = 4$, biologically independent repeats). **b**, ABI2 suppresses ABA-induced OST1 phosphorylation. Protoplasts were co-transfected with *ABI2-HA* and *OST1-Flag* followed by treatment with 1 μM SCREW1 before adding 1 μM ABA. Proteins were separated with Mn^{2+}-Phos-tag (top two) or regular SDS-PAGE (bottom three) and detected with anti-HA or anti-Flag antibodies. The protein loading is shown by CBB staining for RBC. Signal intensities of bands from four independent immunoblots were analysed by ImageJ (bottom). The relative phosphorylation of OST1 represents the ratio of phosphorylated to unphosphorylated OST1. Data are shown as mean ± s.d. ($n = 4$, biologically independent repeats). **c**, SCREW1 suppresses ABA-induced OST1 phosphorylation in a dosage-dependent manner. Protoplasts were transfected with *OST1-Flag* followed by treatments with 0, 10, 100 or 1,000 nM SCREW1 for 5 min before adding 1 μM ABA for another 5 min. Proteins were separated with Mn^{2+}-Phos-tag (top two) and regular SDS-PAGE (middle two) and detected with anti-Flag antibodies. The protein loading is shown by CBB staining for RBC. Signal intensities of bands from four independent immunoblots were analysed by ImageJ. The relative phosphorylation of OST1 represents the ratio of phosphorylated to unphosphorylated OST1. Data are shown as mean ± s.d. ($n = 4$, biologically independent repeats). **d**, NUT interacts with ABI1 in protoplasts. Protoplasts were co-transfected with *ABI1-HA* and *NUT-Flag* or a control vector. Proteins were immunoprecipitated with anti-Flag agarose beads and detected with anti-HA or anti-Flag antibodies (top two). Proteins before IP are shown as input controls (bottom two). **e**, GST-NUT_{CD} interacts with ABI1 *in vitro*. GST or GST-NUT_{CD} proteins were immobilized on glutathione sepharose beads and incubated with His-ABI1-HA followed by immunoblotting with anti-HA antibodies (top). The protein loading is shown by CBB (bottom). Experiments were repeated three times with similar results. Data were analysed by one-way (**b**, **c**) or two-way (**a**) ANOVA followed by Tukey's test. Exact *P* values are provided in the graphs and Supplementary Table 3.

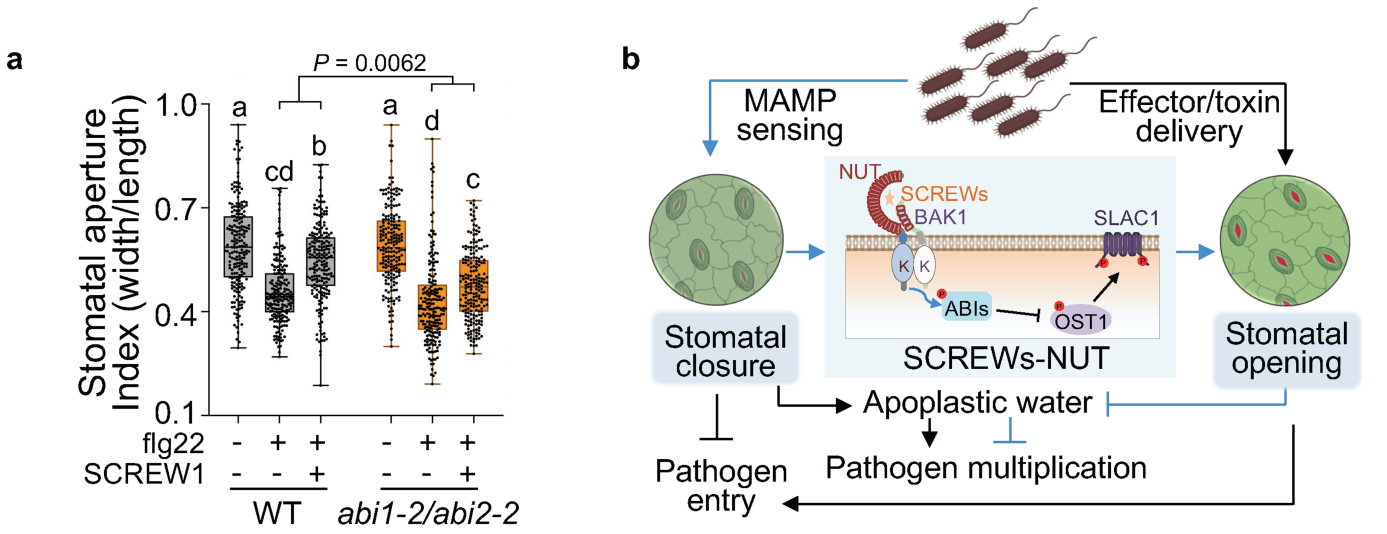

Extended Data Fig. 12 | SCREW1 suppresses flg22-induced stomatal closure through the ABI–OST1 module. a, ABI1 and ABI2 are required for SCREW1 suppression of flg22-induced stomatal closure. The stomatal apertures from epidermal peels of WT and *abi1-2/abi2-2* were measured after treatment without or with 1 μM SCREW1, 1 μM flg22, or a combination of SCREW1 and flg22 for 2 h. Data are shown as the box plots with the interquartile range as the upper and lower confines, minima and maxima as whiskers, and the median as a solid line ($n = 202$, the number of stomata). The different letters denote a statistically significant difference ($P < 0.05$, two-way ANOVA followed by the Tukey's test). The effect of SCREW1 on flg22-induced stomatal closure in WT and *abi1-2/abi2-2* was compared by a two-sided Student's *t*-test. The experiment was repeated three times with similar results. Exact *P* values are provided in the graph and Supplementary Table 3. **b**, A model of SCREW–NUT in protecting plants against infections via promoting stomatal reopening and reducing apoplastic water levels. MAMP perception by PRRs induces stomatal closure to limit pathogen entry. Inevitably, stomatal closure increases the apoplastic water levels and creates aqueous habitats favourable for pathogen multiplication. To counteract, MAMP–PRR signalling induces the expression of SCREWs and *NUT*. Upon SCREW perception, NUT complexes with BAK1 and promotes stomatal reopening via regulating the ABI–OST1–SLAC1 phosphorylation module, thereby increasing water loss and reducing apoplastic water levels to prevent the pathogen colonization. To invade hosts, pathogens deliver effectors or toxins, some of which can open stomata. The blue lines indicate SCREW–NUT induction and function in plant immunity revealed in this study.

nature research

Corresponding author(s): Libo Shan

Last updated by author(s): Feb 28, 2022

Reporting Summary

Nature Research wishes to improve the reproducibility of the work that we publish. This form provides structure for consistency and transparency in reporting. For further information on Nature Research policies, see our Editorial Policies and the Editorial Policy Checklist.

Statistics

For all statistical analyses, confirm that the following items are present in the figure legend, table legend, main text, or Methods section.

n/a	Confirmed	
☐	☒	The exact sample size (*n*) for each experimental group/condition, given as a discrete number and unit of measurement
☐	☒	A statement on whether measurements were taken from distinct samples or whether the same sample was measured repeatedly
☐	☒	The statistical test(s) used AND whether they are one- or two-sided *Only common tests should be described solely by name; describe more complex techniques in the Methods section.*
☒	☐	A description of all covariates tested
☐	☒	A description of any assumptions or corrections, such as tests of normality and adjustment for multiple comparisons
☐	☒	A full description of the statistical parameters including central tendency (e.g. means) or other basic estimates (e.g. regression coefficient) AND variation (e.g. standard deviation) or associated estimates of uncertainty (e.g. confidence intervals)
☐	☒	For null hypothesis testing, the test statistic (e.g. *F*, *t*, *r*) with confidence intervals, effect sizes, degrees of freedom and *P* value noted *Give P values as exact values whenever suitable.*
☒	☐	For Bayesian analysis, information on the choice of priors and Markov chain Monte Carlo settings
☒	☐	For hierarchical and complex designs, identification of the appropriate level for tests and full reporting of outcomes
☒	☐	Estimates of effect sizes (e.g. Cohen's *d*, Pearson's *r*), indicating how they were calculated

Our web collection on statistics for biologists contains articles on many of the points above.

Software and code

Policy information about availability of computer code

Data collection	ImageJ bundled with 64-bit Java 1.8.0_172 for western gel blot analysis; Biacore T200 control software (version 2.0.2) and Evaluation software (version 3.1) for SPR assays; CEZ-2200 patch-clamp amplifier (Nihon Kohden, Japan) and pCLAMP 8.1 software (Molecular Devices, Inc., USA) for Whole-cell S-type anion current recordings; GloMax® Navigator Microplate Luminometer for ROS and calcium burst; MEGAX and iTOL for construction and visualization phylogenetic tree; JEOL1200Ex electron microscope for transmission electron microscopy analysis, CLUSTALW and (https://www.genome.jp/tools-bin/clustalw) and ESPript3 (espript.ibcp.fr) for sequence alignment and visualization.
Data analysis	Confocal images for Arabidopsis were analyzed with Leica TCS SP8 confocal laser scanning microscope (Germany). Statistical analysis was performed with Microsoft Excel 2016, IBM SPSS Statistics 26, or Graphpad Prism 8.0.1.

For manuscripts utilizing custom algorithms or software that are central to the research but not yet described in published literature, software must be made available to editors and reviewers. We strongly encourage code deposition in a community repository (e.g. GitHub). See the Nature Research guidelines for submitting code & software for further information.

Data

Policy information about availability of data

All manuscripts must include a data availability statement. This statement should provide the following information, where applicable:

- Accession codes, unique identifiers, or web links for publicly available datasets
- A list of figures that have associated raw data
- A description of any restrictions on data availability

The data supporting the findings of this study are available within the paper and its Supplementary Information files (uncropped blots and gel images, primers, peptides, and exact P values). Source Data (graphs) for Figs. 1-4 and Extended Data Figs. 1–12 are provided with the paper. The sequences of proteins were

obtained from TAIR (https://www.arabidopsis.org/), UnniProt (https://www.uniprot.org/), NCBI (https://www.ncbi.nlm.nih.gov/), and Phytozome (https://phytozome-next.jgi.doe.gov/). The protein structure were obtained from AlphaFold Protein Structure Database (https://alphafold.ebi.ac.uk/).

Field-specific reporting

Please select the one below that is the best fit for your research. If you are not sure, read the appropriate sections before making your selection.

☒ Life sciences ☐ Behavioural & social sciences ☐ Ecological, evolutionary & environmental sciences

For a reference copy of the document with all sections, see nature.com/documents/nr-reporting-summary-flat.pdf

Life sciences study design

All studies must disclose on these points even when the disclosure is negative.

Sample size	Sample size was determined based on previous publications on similar experiments to ensure confident statistical analyses Pst, Botrytis virulence and ROS burst assays: Ma, Xiyu, et al. "Ligand-induced monoubiquitination of BIK1 regulates plant immunity." Nature 581.7807 (2020): 199-203. Stomata movement assays: Rodrigues, Olivier, et al. "Aquaporins facilitate hydrogen peroxide entry into guard cells to mediate ABA-and pathogen-triggered stomatal closure." Proceedings of the National Academy of Sciences 114.34 (2017): 9200-9205. Growth inhibition: Hou, Shuguo, et al. "The secreted peptide PIP1 amplifies immunity through receptor-like kinase 7." PLoS pathogens 10.9 (2014): e1004331. Aphid bioassays: Lei, Jiaxin, et al. "BOTRYTIS-INDUCED KINASE1 modulates Arabidopsis resistance to green peach aphids via PHYTOALEXIN DEFICIENT4." Plant physiology 165.4 (2014): 1657-1670. Gene expression: Yu, Xiao, et al. "Orchestration of processing body dynamics and mRNA decay in Arabidopsis immunity." Cell reports 28.8 (2019): 2194-2205. FRK1 reporter assay: Li, Bo, et al. "Phosphorylation of trihelix transcriptional repressor ASR3 by MAP KINASE4 negatively regulates Arabidopsis immunity." The Plant Cell 27.3 (2015): 839-856. atch-clamp experiments: Takahashi, Yohei, et al. "MAP3Kinase-dependent SnRK2-kinase activation is required for abscisic acid signal transduction and rapid osmotic stress response." Nature communications 11.1 (2020): 1-12. Stomatal conductance: Freeman, Brian C., and Gwyn A. Beattie. "Bacterial growth restriction during host resistance to Pseudomonas syringae is associated with leaf water loss and localized cessation of vascular activity in Arabidopsis thaliana." Molecular plant-microbe interactions 22.7 (2009): 857-867.
Data exclusions	No data were excluded from analyses in the experiments
Replication	All experiments were successfully repeated at least two or three times, and the number of independent experiments or biological replicates is indicated in the figure legends.
Randomization	Plants were randomly assigned to the treatment and control groups with no formal randomization techniques.
Blinding	Investigators were not blinded to plant genotypes during experiments. The research materials are plants so the blinding design is not applicable to this system. Experiment results are not subjective.

Reporting for specific materials, systems and methods

We require information from authors about some types of materials, experimental systems and methods used in many studies. Here, indicate whether each material, system or method listed is relevant to your study. If you are not sure if a list item applies to your research, read the appropriate section before selecting a response.

Materials & experimental systems

n/a	Involved in the study
☐	☒ Antibodies
☐	☒ Eukaryotic cell lines
☒	☐ Palaeontology and archaeology
☐	☒ Animals and other organisms
☒	☐ Human research participants
☒	☐ Clinical data
☒	☐ Dual use research of concern

Methods

n/a	Involved in the study
☒	☐ ChIP-seq
☒	☐ Flow cytometry
☒	☐ MRI-based neuroimaging

Antibodies

Antibodies used	Commercial antibodies used: Anti-HA-Peroxidase, Roche, Cat# 12013819001, clone 3F10, Dilution 1: 2,000. Anti-FLAG-Peroxidase, Sigma-Aldrich, Cat# A8592, clone M2, Dilution 1: 2,000. Anti-GFP, Roche, Cat# 11814460001, mix of clone 7.1 and 13.1, Dilution 1: 2,000.

Anti-FLAG M2 Affinity gel, Sigma-Aldrich, Cat# 2220, clone M2.
Anti-pERK1/2 antibodies, Cell Signaling, Cat# 9101, Polyclone, Dilution 1: 2,000.
HRP-labeled Streptavidin, Thermo Fisher, Cat# N100, Dilution 1: 5,000.
Anti-PR1, Agrisera, Cat#AS10687, Plolyclone, Dilution 1: 2,000.
Anti-Rabbit IgG, HRP-linked antibody, Cell Signaling, Cat # 7074, Polyclone, Dilution 1: 10,000.
Anti-Mouse IgG, HRP-linked antibody, Cell Signaling, Cat# 7076 , Polyclone, Dilution 1: 10,000.
Custom-made antibodies used:
Anti-BAK1, Polyclone, Dilution 1:2000.
Anti-FLS2, Polyclone, Dilution 1:2000.

Validation

Validation statements, relevant citations of commercial primary antibodies are available from manufacturers:
Anti-HA-Peroxidase, Roche, Cat # 12013819001, clone 3F10. https://www.sigmaaldrich.com/catalog/product/roche/12013819001?lang=en&region=US
Anti-FLAG-Peroxidase, Sigma-Aldrich, Cat # A8592, clone M2. https://www.sigmaaldrich.com/catalog/product/sigma/a8592?lang=en&region=US
Anti-GFP, Roche, Cat # 11814460001, mix of clone 7.1 and 13.1. https://www.sigmaaldrich.com/catalog/product/roche/11814460001?lang=en&region=US
Anti-FLAG M2 Affinity gel, Sigma-Aldrich, Cat # 2220, clone M2. https://www.sigmaaldrich.com/catalog/product/sigma/a2220?lang=en&region=US
Anti-pERK1/2, Cell Signaling, Cat # 9101. https://www.cellsignal.com/products/primary-antibodies/phosphop44-42-mapk-erk1-2-thr202-tyr204-antibody/9101
HRP-labeled Streptavidin, Thermo Fisher, Cat# N100, https://www.thermofisher.com/order/catalog/product/N100
Anti-PR1, Agrisera, Cat#AS10687, Plolyclone, Confirmed activity (Arabidopsis thaliana, Hordeum vulgare, Nicotiana bentamiana, Spinacia oleracea, Solanum lycopersicum, Triticum aestivum, Vitis vinifera, Zea mays) https://www.agrisera.com/en/artiklar/pr-1-pathogenesis-related-protein-1.html
Anti-Rabbit IgG, HRP-linked antibody, Cell Signaling, Cat # 7074. https://www.cellsignal.com/products/secondary-antibodies/anti-rabbit-igg-hrp-linked-antibody/7074
Anti-Mouse IgG, HRP-linked antibody, Cell Signaling, Cat # 7076. https://www.cellsignal.com/products/secondary-antibodies/anti-mouse-igg-hrp-linked-antibody/7076
Anti-BAK1, custom-made, Validation in the reference: https://academic.oup.com/plphys/article/180/1/543/6117761?login=true
Anti-FLS2, custom-made, Validation in the reference:https://www.science.org/doi/full/10.1126/science.1204903?casa_token=-P4m5yl34uQAAAAA%3AC0awfxYV0ZvfxIw_LuOhsPs140aF-URIlvVRknSEs1X5PLS6A6zaCTVELym6VmP-RpIQHTXGH1wMZtk

Eukaryotic cell lines

Policy information about cell lines

Cell line source(s)	SF9 cells, Thermo Fisher Scientific, Cat#: 11496015
Authentication	SF9 cells were not further authenticated by authors in this study.
Mycoplasma contamination	SF9 cells were not tested for mycoplasma contamination by authors in this study.
Commonly misidentified lines (See ICLAC register)	No commonly misidentified cell lines were used.

Animals and other organisms

Policy information about studies involving animals; ARRIVE guidelines recommended for reporting animal research

Laboratory animals	Green peach aphids (Myzus persicae) used in this study are a tobacco (Nicotiana tabacum)-adapted red lineage which were maintained on cabbage (Brassica oleracea). Both adults and nymphs were female used in our experiments.
Wild animals	The study did not involve wild animals.
Field-collected samples	The study did not involve samples collected from field.
Ethics oversight	No ethical approval was required for nymphs of aphid (Myzus persicae).

Note that full information on the approval of the study protocol must also be provided in the manuscript.